

Unraveling the mechanism of the hydrodeoxygenation of propionic acid over a Pt (111) surface in vapor and liquid phases

Wenqiang Yang¹, Rajadurai Vijay Solomon¹, Jianmin Lu¹, Osman Mamun¹, Jesse Q. Bond², and Andreas Heyden^{1,*}

¹ *Department of Chemical Engineering, University of South Carolina,
301 S. Main Street, Columbia, SC 29208, USA.*

² *Department of Biomedical and Chemical Engineering, Syracuse University,
329 Link Hall, Syracuse, New York 13244, USA*

*Corresponding author email: heyden@cec.sc.edu

phone: +1-803-777-5025

Abstract

Microkinetic models based on first principles calculations have been developed for the vapor and liquid phase hydrodeoxygenation of propionic acid over a Pt (111) surface. Calculations suggest that decarboxylation does not occur at an appreciable rate. In the vapor phase, decarbonylation products, propanal and propanol are all produced at similar rates. However, in both liquid water and 1,4-dioxane, propanol and propanal are favored over decarbonylation products. While a condensed phase can shift the reaction rate and selectivity significantly, the dominant pathways towards the various products are hardly affected. Only for propanal production do we observe a shift in mechanism. At 473 K, the propionic acid conversion rate is increased by one order of magnitude in liquid 1,4-dioxane relative to the gas phase. In liquid water, the conversion rate is similar to the vapor phase since adsorbed propionic acid blocks a large fraction of the surface sites.

Keywords: Propionic acid, Hydrodeoxygenation mechanism, Propanol, Propionaldehyde, Microkinetic modeling, Solvent effect, Lateral interaction

1 Introduction

During the past decades, increasing consumption of fossil fuels has caused growing environmental and climate concerns. As a result, many efforts have been devoted to renewable energy resources, such as wind, solar, geothermal, hydropower and biomass. Among them, biomass is the only renewable carbon source and thus one of the most promising alternative energy sources for liquid fuel and chemical production[1, 2]. Triglycerides, the main constituent of vegetable oils and animal fats, can be used to produce first generation biofuels such as fatty acid methyl and ethyl esters (FAMES) through a process called transesterification[3-5]. But FAMES have their own disadvantages, such as high viscosity, poor oxidation stability, low energy density, and high cloud point temperature[3, 4]. Therefore, conversion of triglycerides and their fatty acids to hydrocarbons with similar or identical properties to conventional fossil fuels, known as “green diesel”, is of significant academic and industrial interest[6]. In recent years, hydrodeoxygenation (HDO), a process to convert triglycerides or fatty esters/acids obtained from lipid-rich biomass feedstock into liquid hydrocarbon fuels, has gained attention[2, 7]. However, the conventional heterogeneous catalysts used for the HDO process such as sulfided NiMo/Al₂O₃ and CoMo/Al₂O₃ have various drawbacks[5, 8]. For instance, short catalyst life times and high sulfur content in the final product have been found[5, 8]. To overcome the limitations of using conventional sulfided catalysts in biomass processing, new catalysts must be developed, which requires a better understanding of the HDO mechanism of triglycerides and organic esters/ acids on metal catalysts.

Recently, we have studied the HDO of an organic acid model molecule (propionic acid) to C₂ hydrocarbons on different Pd and Ru transition metal surfaces based on first-principle calculations[9-14]. We found that the HDO of propionic acid is mainly associated with two major reaction mechanisms: (1) decarbonylation (DCN) and (2) decarboxylation (DCX). For all the metal surfaces investigated in our previous studies, the DCN path is favored over the DCX pathway. Besides DCN and DCX pathways, alcohols and aldehydes can also be produced during the HDO of propionic acid. For example, Chen et al.[15] found that Ru/C has a high selectivity to propanol in the HDO of propionic acid at a temperatures of around 400 K and high H₂ partial pressure (>20 bar). Unfortunately, to the best of our knowledge, there is little work reporting the mechanisms of alcohol and aldehyde production in the HDO of propionic acid. In order to gain more insights into the mechanisms of the HDO of organic acids (such as propionic acid) on transition metal surfaces and to guide the design of metal catalysts, it is necessary to study multiple metal surfaces and

include as many reaction mechanisms as possible in the reaction network. Pt catalysts have long been shown to have a high activity towards HDO reactions [16-19]. Interestingly, production of multiple reaction products appears favorable. For instance, Rachmady and Vannice have studied the vapor phase acetic acid hydrogenation over supported Pt catalysts and observed various products such as CO, CH₄, ethanol, ethane and ethyl acetate [19]. Similarly, Olcay et al. studied the aqueous-phase hydrogenation of acetic acid over transition metal catalysts and observed both ethanol and alkane products over Pt catalysts [20]. In contrast, Lugo-José et al. studied the vapor phase HDO of propanoic acid over Pt catalysts and found essentially 100% selectivity towards DCN and DCX products [21]. Clearly, the reaction conditions and environment appear to strongly affect the product selectivity and thus, Pt metal catalysts are an ideal model system for identifying rate and selectivity determining steps for the HDO of propionic acid towards DCN, DCX, alcohol and aldehyde production in various reaction environments.

In regards to solvent effects, a few studies have reported a significant effect of a solvent on the reaction mechanism, activity and selectivity of HDO reactions [10, 14, 22, 23]. For instance, Hoelderich et al. studied the deoxygenation of oleic acid (C18) over Pd/C catalyst in liquid water and found that water can change the selectivity towards C17 hydrocarbons by up to 20% [24]. Similarly, Behtash et al. found that in liquid water the rate of DCX is increased for the HDO of propionic acid and becomes competitive to the DCN over both Pd (111) and Pd (211) surfaces [10, 14]. Due to the increased activity of the Pd surface in liquid water for C-CO₂ bond cleavage, activation of the C-C bond by dehydrogenation (C-H bond cleavage) prior to C-C bond cleavage (a necessary step in the vapor phase) was found to be unnecessary in liquid water. Finally, Mamun et al. studied the solvent effect on the hydrodeoxygenation of levulinic acid over Ru catalysts and observed rate increases of 2-4 orders of magnitude in liquid water relative to 1,4-dioxane [25]. Thus, in this paper, we investigated the HDO mechanisms of propionic acid over Pt (111) under both gas and liquid phase conditions. Water and 1,4-dioxane have been selected as solvents as they are among the most often used solvents in both the academic and industrial communities. We aimed at determining the dominant reaction pathways and identifying the rate- and selectivity-controlling steps for the HDO of propionic acid under both vapor and liquid phase conditions. The solvent effect on the full microkinetic modelling results, such as reaction orders, apparent activation energies and turnover frequencies (TOFs) have also been discussed.

2 METHODS

2.1 Computational Methods.

All gas phase calculations were carried out using the Vienna Ab Initio Simulation Package (VASP)[26, 27] based on density functional theory (DFT) with the projector augmented wave (PAW) method[28]. The generalized gradient approximation (GGA) with the Perdew and Wang 1991 functional (PW91) was used to treat exchange correlation effects[29, 30]. An energy cutoff of 400 eV is used for all DFT calculations and the energy convergence criterion was set to 10^{-7} eV. All structures were relaxed until the Hellmann-Feynman force on each atom were smaller than $0.01 \text{ eV } \text{\AA}^{-1}$. The optimized lattice constant of a Pt unit cell (3.976\AA) is in good agreement with the reported experimental value of 3.912\AA [31] and has been used for the construction of the Pt (111) surface model. To simulate the Pt surface, a $3 \times 2\sqrt{3}$ Pt (111) surface model was constructed with four Pt atom layers separated by a 15\AA vacuum gap. The dipole correction was applied to the direction perpendicular to the surface. For all surface calculations, the bottom two layers were fixed to their bulk positions while the top two layers were fully relaxed in all directions. In the vibrational frequency calculations, however, all metal atoms were fixed at their optimized positions. The Brillouin zone integration was sampled by $4 \times 4 \times 1$ k-points for the surface using the Monkhorst-Pack scheme[32]. In order to precisely locate the transition states of the elementary reactions, a combination of the climbing image nudged elastic band (CI-NEB) method and the dimer method was used[33-36]. It should be noted that frequencies below 100 cm^{-1} were shifted to 100 cm^{-1} for the calculation of partition functions in order to minimize the errors associated with the harmonic approximation for small frequencies[12].

The solvent effect of a liquid is investigated using the implicit solvation model for solid surfaces (iSMS) method. Information about the iSMS method has recently been published, [23] and a convergence plot of the iSMS method with system size is provided in Figure S9 in the supporting information. The key point of this model is to include the long-range metal interactions through periodic-slab calculations within the framework of DFT calculations in the absence of a solvent and to consider the effect of the liquid as a localized perturbation that can be described by cluster models embedded in an implicit continuum solvent. We define a free energy function for an adsorbed surface intermediate on a periodic metal slab in liquid, $G_{\text{surface+intermediate}}^{\text{liquid}}$, using a simple subtraction scheme as follows:

$$G_{\text{surface+intermediate}}^{\text{liquid}} = G_{\text{surface+intermediate}}^{\text{vacuum}} + (G_{\text{cluster+intermediate}}^{\text{liquid}} - E_{\text{cluster+intermediate}}^{\text{vacuum}}) \quad (1)$$

where $G_{surface+intermediate}^{vacuum}$ is the DFT free energy (harmonic approximation for vibrational contributions) of the surface slab model in the absence of a solvent, $G_{cluster+intermediate}^{liquid}$ is the free energy of a metal cluster in the liquid built by removing selected metal atoms from the periodic slab model and removing the periodic boundary conditions (vibrational contributions are not considered), while $E_{cluster+intermediate}^{vacuum}$ is the DFT energy of the same cluster model without the solvent. The COSMO-RS implicit solvation model was used to compute $G_{cluster+intermediate}^{liquid}$ through the COSMOtherm program. Thermodynamic properties of the solvents are obtained from the COSMOtherm database at the BP/TZVP level of theory. For all the remaining structures, COSMO-RS input files have been generated from the COSMO calculations at the same level of theory. Given the uncertainty in the solvent parameters for the Pt metal atoms, the solvent calculations were repeated with a cavity radius that is $\pm 10\%$ of the default Pt cavity. In this way, we study the sensitivity of our liquid phase results with respect to the most important Pt solvent parameter.

2.2 Microkinetic Modeling

Adsorption free energies of all intermediates, G_{ads} , have been calculated with a universal reference based on the following equations:

$$G_{ads} = G_{slab+intermediate} - G_{slab} - N_C \times E_C - N_H \times E_H - N_O \times E_O \quad (2)$$

$$E_H = 0.5 \times E_{H_2} \quad (3)$$

$$E_C = E_{CH_4} - 2 \times E_{H_2} \quad (4)$$

$$E_O = E_{H_2O} - E_{H_2} \quad (5)$$

where $G_{slab+intermediate}$ is the free energy of the intermediate on the surface slab, G_{slab} is the free energy of the clean surface slab, and E_{CH_4} , E_{H_2O} , E_{H_2} are the energy of the CH_4 , H_2O and H_2 molecules, respectively. N_C , N_H and N_O are the number of C, H and O atoms in the intermediate. Based on the adsorption free energy defined above, the reaction energy and activation energy barrier can be calculated using the following equations:

$$\Delta G_i^{rxn} = \sum_j v_{ij} \times G_{ads,j}^i \quad (6)$$

$$\Delta G_i^\ddagger = G_{ads,i}^\ddagger - \sum G_{ads,i}^R \quad (7)$$

with ΔG_i^{rxn} and ΔG_i^\ddagger being the reaction free energy and activation free energy of reaction step i , respectively. While v_{ij} and $G_{ads,j}^i$ are the stoichiometry coefficient and adsorption free

energy of intermediates j in reaction step i , respectively. Finally, $G_{ads,i}^\ddagger$ and $G_{ads,i}^R$ are the adsorption free energy of the transition state and the sum of the adsorption free energies of the reactant of reaction step i , respectively.

For surface reactions, the forward reaction rate constant (k_{for}) can be calculated according to the transition state theory as,

$$k_{for} = \frac{k_B T}{h} e^{-\frac{\Delta G^\ddagger}{k_B T}} \quad (8)$$

where k_B is the Boltzmann constant, h is Planck constant, T is the reaction temperature in Kelvin, and ΔG^\ddagger is the zero-point corrected activation barrier for the forward reaction obtained from DFT calculations. For adsorption processes, the reaction rate constant can be approximated through collision theory with a sticking coefficient of 1,

$$k_{for} = \frac{1}{N_0 \sqrt{2\pi m_A k_B T}} \quad (9)$$

where N_0 is the number of sites per surface area ($1.454 \times 10^{19} \text{ m}^{-2}$) and m_A denotes the molecular weight of adsorbent A. The reverse reaction rate constant (k_{rev}) is determined from the thermodynamic equilibrium constant K ,

$$K = \frac{k_{for}}{k_{rev}} \quad (10)$$

In the presence of solvents, the free energy of reaction and activation barrier were calculated as,

$$\Delta G_{solvent,i}^\ddagger = G_{gas,i}^\ddagger + G_{TS(solv)} - G_{IS(solv)} \quad (11)$$

$$\Delta G_{solvent,i}^{rxn} = G_{gas,i}^{rxn} + G_{FS(solv)} - G_{IS(solv)} \quad (12)$$

where $G_{IS(solv)}$, $G_{FS(solv)}$, and $G_{TS(solv)}$ are the solvation free energies of the reactants, transition state and products of reaction step i , respectively, which were obtained from the COSMO-RS calculations.

With all the forward and reverse reaction rate constants specified, a mean-field microkinetic model was built for the normalized number of surface species i per surface metal atoms[37]. The surface coverage of each species is equal to the number of sites occupied by the species (see Table S3 in the SI) times the normalized number of surface species i per surface metal atoms. Steady state surface coverages and rates are obtained by using the Matlab ODE solver ode15s. No assumptions were made regarding the rate controlling steps in building our models.

2.3 Lateral interaction effects

The mean-field approximation of microkinetic models is typically derived under the assumption of no lateral adsorbate-adsorbate interactions. In particular, strong adsorbate-adsorbate attraction can lead to island formation which leads to an overestimation of the rate predicted by the mean-field approximation. At the same time, slight adsorbate-adsorbate repulsion can still be accommodated by mean-field models that consider the repulsive interaction within the free energy expression[38]. Without considering any lateral interactions, results from our mean-field microkinetic model showed that CO and H cover more than 95% of the Pt surface and the fraction of available free sites becomes exceedingly small. Since both adsorbed CO and H display significant lateral (repulsive) interactions, we should consider these interactions in our models. Here, we used a linear lateral interaction model for describing the effects of any high-coverage surface species (i.e., CO and H) on the free energy of any surface species in the microkinetic model. To describe the lateral interaction effect on activation barriers, we assumed that the transition states are affected as half the reactant and half the product:

$$G_{ads}^i(\theta_j) = G_{ads}^i(0) + a_{i,j} * \theta_j \quad (13)$$

$$G_{ads}^i(\theta_1, \dots, \theta_n) = G_{ads}^i(0) + \sum_{j \neq i}^n a_{i,j} * \theta_j \quad (14)$$

$$G_a^k(\theta_1, \dots, \theta_n) = G_a^k(0) + 0.5(G_{rxn}^k(0) - G_{rxn}^k(\theta_1, \dots, \theta_n)) \quad (15)$$

where $G_{ads}^i(0)$ and $G_{ads}^i(\theta_j)$ are adsorption energies of species i on the clean surface and surface with θ_j sites covered by species j , respectively. $a_{i,j}$ is the lateral interaction coefficient of species j to species i , and $G_a^k(\theta_1, \dots, \theta_n)$ and $G_{rxn}^k(\theta_1, \dots, \theta_n)$ are the activation and reaction free energy of step k with a surface covered by species i with coverage θ_i , respectively. All adsorption energies are calculated for all species at zero coverage and a coverage of 0.25 ML of CO and H. Table S4 in the SI lists all the $a_{i,j}$ parameters.

3 Results and Discussion

A detailed reaction network for the HDO of propionic acid on Pt (111) along with the intermediates involved in various elementary reaction steps is shown in Fig. 1. The reaction network of the DCN and DCX in Fig. 1a is identical to our previous study on the HDO of propionic acid over Pd and Ru catalysts[9, 12, 13] while Fig. 1b shows the reaction network of propanol and propionaldehyde production. It is to be noted that we did not include the water-gas shift reaction in our reaction network that is able to reduce the CO partial pressure in the reactor. The water-gas

shift reaction hardly occurs on Pt (111) but is believed to be catalyzed by Pt-oxide support interface sites[39, 40]. Thus, in the absence of a meaningful active site model for the water-gas shift, we are required to set the CO partial pressure to a practical value that leads to CO surface coverages and modeling results comparable to experimental observations. Fortunately, we found that our microkinetic modeling results are not very sensitive to the CO partial pressure due to the inclusion of lateral surface species interactions with CO in our microkinetic models (see section 3.2). Table 1 gives the reaction free energies and activation free energy barriers at a temperature of 473 K. The solvent effects of water and 1,4-dioxane are treated as corrections to the reaction and activation free energies, which are also provided in Table 1. In the following section, we will discuss the effects of solvents on various elementary reaction steps. Then, we will discuss the results of our microkinetic reactor model under both gas phase and liquid phase conditions, which includes the turnover frequency (TOF), the dominant pathways for various products, selectivity towards different products and the effects of solvent on them. Results from our sensitivity analysis, which includes degree of rate control, degree of thermodynamic rate control, and degree of selectivity control, will be discussed thereafter. Finally, reaction orders and apparent activation energies under both gas and liquid phases will be reported.

Table 1 Reaction free energies in eV of all elementary reaction steps in the HDO of PAc on a Pt (111) surface at a temperature of 473 K in the vapor phase and in the presence of liquid water and 1, 4-dioxane. The number of * signifies the number of adsorption sites.

| # | Reaction | Gas | | Water | | 1-4-dioxane | |
|----|--|-------------------------|---------------------|-------------------------------|---------------------------|-------------------------------|---------------------------|
| | | ΔG_{rxn} | ΔG^\ddagger | $\Delta\Delta G_{\text{rxn}}$ | $\Delta\Delta G^\ddagger$ | $\Delta\Delta G_{\text{rxn}}$ | $\Delta\Delta G^\ddagger$ |
| 0 | $\text{CH}_3\text{CH}_2\text{COOH}(\text{g}) + * \rightarrow \text{CH}_3\text{CH}_2\text{COOH}^*$ | 0.79 | N/A | -0.26 | N/A | -0.20 | N/A |
| 1 | $\text{CH}_3\text{CH}_2\text{COOH}^* + 3* \rightarrow \text{CH}_3\text{CH}_2\text{CO}^{***} + \text{OH}^*$ | 0.52 | 0.70 | 0.08 | 0.06 | 0.08 | 0.05 |
| 2 | $\text{CH}_3\text{CH}_2\text{COOH}^* + 2* \rightarrow \text{CH}_3\text{CHCOOH}^{**} + \text{H}^*$ | -0.21 | 0.72 | -0.03 | -0.06 | 0.02 | -0.02 |
| 3 | $\text{CH}_3\text{CH}_2\text{CO}^{***} \rightarrow \text{CH}_3\text{CH}_2^* + \text{CO}^* + *$ | -0.74 | 1.47 | -0.11 | -0.06 | -0.08 | -0.05 |
| 4 | $\text{CH}_3\text{CH}_2\text{CO}^{***} \rightarrow \text{CH}_3\text{CHCO}^{**} + \text{H}^*$ | -0.29 | 0.71 | -0.05 | -0.09 | -0.02 | -0.04 |
| 5 | $\text{CH}_3\text{CHCOOH}^{**} + * \rightarrow \text{CH}_3\text{CHCO}^{**} + \text{OH}^*$ | 0.44 | 0.78 | 0.06 | 0.11 | 0.04 | 0.06 |
| 6 | $\text{CH}_3\text{CHCOOH}^{**} + 2* \rightarrow \text{CH}_2\text{CHCOOH}^{***} + \text{H}^*$ | -0.29 | 0.67 | 0.03 | -0.02 | 0.02 | 0.01 |
| 7 | $\text{CH}_3\text{CHCOOH}^{**} + 2* \rightarrow \text{CH}_3\text{CCOOH}^{***} + \text{H}^*$ | -0.10 | 0.74 | 0.01 | 0.02 | -0.01 | -0.01 |
| 8 | $\text{CH}_3\text{CHCO}^{**} + * \rightarrow \text{CH}_3\text{CH}^{**} + \text{CO}^*$ | -0.54 | 0.84 | -0.10 | 0.01 | -0.05 | 0.01 |
| 9 | $\text{CH}_3\text{CHCO}^{**} + 2* \rightarrow \text{CH}_3\text{CCO}^{***} + \text{H}^*$ | -0.31 | 0.65 | -0.01 | -0.02 | 0.01 | 0.00 |
| 10 | $\text{CH}_3\text{CHCO}^{**} + 2* \rightarrow \text{CH}_2\text{CHCO}^{***} + \text{H}^*$ | 0.06 | 0.87 | -0.03 | -0.09 | 0.00 | -0.04 |
| 11 | $\text{CH}_2\text{CHCOOH}^{***} + * \rightarrow \text{CH}_2\text{CHCO}^{***} + \text{OH}^*$ | 0.78 | 1.47 | 0.00 | 0.07 | 0.02 | 0.05 |
| 12 | $\text{CH}_2\text{CHCOOH}^{***} + * \rightarrow \text{CHCHCOOH}^{***} + \text{H}^*$ | -0.07 | 0.77 | -0.04 | -0.09 | -0.03 | -0.04 |
| 13 | $\text{CH}_3\text{CCOOH}^{***} + * \rightarrow \text{CH}_3\text{CCO}^{***} + \text{OH}^*$ | 0.23 | 0.77 | 0.04 | 0.06 | 0.06 | 0.06 |
| 14 | $\text{CH}_3\text{CCO}^{***} \rightarrow \text{CH}_3\text{C}^* + \text{CO}^* + *$ | -1.18 | 0.75 | -0.09 | 0.04 | -0.07 | 0.01 |
| 15 | $\text{CH}_2\text{CHCO}^{***} + * \rightarrow \text{CH}_2\text{CH}^{***} + \text{CO}^*$ | -0.89 | 0.69 | -0.09 | 0.00 | -0.06 | 0.00 |
| 16 | $\text{CH}_2\text{CHCO}^{***} + 2* \rightarrow \text{CHCHCO}^{****} + \text{H}^*$ | -0.20 | 0.61 | -0.01 | -0.05 | 0.00 | -0.01 |
| 17 | $\text{CHCHCOOH}^{****} + 2* \rightarrow \text{CHCHCO}^{****} + \text{OH}^*$ | 0.65 | 1.09 | 0.04 | 0.06 | 0.06 | 0.07 |
| 18 | $\text{CHCHCO}^{****} \rightarrow \text{CHCH}^{****} + \text{CO}^*$ | -0.82 | 0.51 | -0.11 | 0.02 | -0.07 | 0.01 |

| | | | | | | | |
|----|---|-------|-------|-------|-------|-------|-------|
| 19 | $\text{CH}_2\text{CH}^{***} + * \rightarrow \text{CHCH}^{***} + \text{H}^*$ | -0.13 | 0.69 | -0.03 | -0.07 | -0.01 | -0.04 |
| 20 | $\text{CH}_2\text{CH}_2^{**} + 2* \rightarrow \text{CH}_2\text{CH}^{***} + \text{H}^*$ | -0.05 | 0.69 | -0.03 | -0.08 | -0.01 | -0.04 |
| 21 | $\text{CH}_2\text{CH}^{***} \rightarrow \text{CH}_2\text{C}^{**} + \text{H}^*$ | -0.38 | 0.38 | 0.00 | -0.03 | 0.00 | -0.01 |
| 22 | $\text{CH}_3\text{C}^* + 2* \rightarrow \text{CH}_2\text{C}^{**} + \text{H}^*$ | 0.27 | 1.06 | -0.02 | -0.09 | 0.00 | -0.05 |
| 23 | $\text{CH}_3\text{CH}^{**} + 2* \rightarrow \text{CH}_2\text{CH}^{***} + \text{H}^*$ | -0.29 | 0.51 | -0.01 | -0.11 | -0.01 | -0.07 |
| 24 | $\text{CH}_3\text{CH}^{**} \rightarrow \text{CH}_3\text{C}^* + \text{H}^*$ | -0.94 | 0.25 | 0.00 | -0.03 | 0.00 | -0.02 |
| 25 | $\text{CH}_3\text{CH}_2^* + 2* \rightarrow \text{CH}_3\text{CH}^{**} + \text{H}^*$ | -0.10 | 0.66 | -0.03 | -0.07 | 0.00 | -0.03 |
| 26 | $\text{CH}_3\text{CH}_3^* + * \rightarrow \text{CH}_3\text{CH}_2^* + \text{H}^*$ | -0.11 | 0.64 | -0.01 | -0.07 | 0.01 | -0.02 |
| 27 | $\text{CH}_3\text{CH}_2^* + 2* \rightarrow \text{CH}_2\text{CH}_2^{**} + \text{H}^*$ | -0.34 | 0.57 | -0.01 | -0.09 | 0.01 | -0.04 |
| 28 | $\text{CH}_3\text{CH}_2\text{COOH}^* + 2* \rightarrow \text{CH}_3\text{CH}_2\text{COO}^{**} + \text{H}^*$ | -0.41 | 0.31 | 0.11 | 0.07 | 0.07 | 0.03 |
| 29 | $\text{CH}_3\text{CH}_2\text{COO}^{**} \rightarrow \text{CH}_3\text{CH}_2^* + \text{CO}_2^*$ | -0.09 | 1.49 | -0.01 | -0.01 | 0.00 | 0.02 |
| 30 | $\text{CH}_3\text{CH}_2\text{COO}^{**} + 2* \rightarrow \text{CH}_3\text{CHCOO}^{***} + \text{H}^*$ | 0.47 | 1.24 | -0.10 | -0.17 | -0.02 | -0.05 |
| 31 | $\text{CH}_3\text{CHCOOH}^{**} + 2* \rightarrow \text{CH}_3\text{CHCOO}^{***} + \text{H}^*$ | 0.27 | 0.75 | 0.04 | 0.01 | 0.03 | 0.01 |
| 32 | $\text{CH}_3\text{CHCOOH}^{**} + 2* \rightarrow \text{CH}_3\text{CH}^{**} + \text{COOH}^{**}$ | -0.04 | 1.42 | -0.04 | -0.01 | -0.02 | -0.02 |
| 33 | $\text{CH}_3\text{CHCOO}^{***} \rightarrow \text{CH}_3\text{CH}^{**} + \text{CO}_2^*$ | -0.66 | 0.95 | 0.06 | 0.09 | 0.02 | 0.04 |
| 34 | $\text{CH}_3\text{CHCOO}^{***} + * \rightarrow \text{CH}_3\text{CCOO}^{***} + \text{H}^*$ | -0.22 | 1.04 | -0.05 | -0.02 | -0.02 | -0.01 |
| 35 | $\text{CH}_3\text{CCOOH}^{***} + * \rightarrow \text{CH}_3\text{CCOO}^{***} + \text{H}^*$ | 0.15 | 0.90 | -0.02 | 0.05 | 0.03 | 0.06 |
| 36 | $\text{CH}_3\text{CCOOH}^{***} + * \rightarrow \text{CH}_3\text{C}^* + \text{COOH}^{**}$ | -0.89 | 1.06 | -0.05 | 0.02 | -0.01 | 0.04 |
| 37 | $\text{CH}_2\text{CHCOOH}^{***} + 2* \rightarrow \text{CH}_2\text{CH}^{***} + \text{COOH}^{**}$ | -0.04 | 1.86 | -0.08 | -0.02 | -0.04 | 0.00 |
| 38 | $\text{CH}_3\text{CCOO}^{***} \rightarrow \text{CH}_3\text{C}^* + \text{CO}_2^* + *$ | -1.38 | 0.79 | 0.11 | 0.18 | 0.03 | 0.09 |
| 39 | $\text{COOH}^{**} \rightarrow \text{CO}_2^* + \text{H}^*$ | -0.35 | 0.45 | 0.14 | 0.04 | 0.07 | 0.01 |
| 40 | $\text{COOH}^{**} \rightarrow \text{CO}^* + \text{OH}^*$ | -0.06 | 0.46 | 0.00 | 0.07 | 0.00 | 0.05 |
| 41 | $\text{H}_2\text{O}^* + * \rightarrow \text{OH}^* + \text{H}^*$ | 0.53 | 0.83 | 0.08 | 0.05 | 0.06 | 0.04 |
| 42 | $\text{CH}_3\text{CH}_3(\text{g}) + * \rightarrow \text{CH}_3\text{CH}_3^*$ | 0.57 | N/A | -0.05 | N/A | -0.06 | N/A |
| 43 | $\text{CH}_2\text{CH}_2(\text{g}) + 2* \rightarrow \text{CH}_2\text{CH}_2^{**}$ | -0.27 | N/A | -0.09 | N/A | -0.05 | N/A |
| 44 | $\text{H}_2\text{O}(\text{g}) + * \rightarrow \text{H}_2\text{O}^*$ | 0.52 | N/A | -0.16 | N/A | -0.10 | N/A |
| 45 | $\text{CO}_2(\text{g}) + * \rightarrow \text{CO}_2^*$ | 0.54 | N/A | -0.09 | N/A | -0.07 | N/A |
| 46 | $\text{CHCH}(\text{g}) + 3* \rightarrow \text{CHCH}^{***}$ | -1.56 | N/A | -0.16 | N/A | -0.07 | N/A |
| 47 | $\text{CO}(\text{g}) + * \rightarrow \text{CO}^*$ | -0.59 | N/A | -0.15 | N/A | -0.10 | N/A |
| 48 | $\text{H}_2(\text{g}) + 2* \rightarrow \text{H}^* + \text{H}^*$ | -0.36 | N/A | 0.01 | N/A | 0.00 | N/A |
| 49 | $\text{CH}_3\text{CHCHO}^{***} \rightarrow \text{CH}_3\text{CHCO}^{**} + \text{H}^*$ | -0.92 | 0.08 | 0.04 | 0.03 | 0.01 | 0.01 |
| 50 | $\text{CH}_3\text{CHCOH}^{***} \rightarrow \text{CH}_3\text{CHCO}^{**} + \text{H}^*$ | -0.26 | 0.60 | 0.00 | 0.00 | -0.01 | -0.01 |
| 51 | $\text{CH}_3\text{CH}_2\text{CHO}^* + 3* \rightarrow \text{CH}_3\text{CH}_2\text{CO}^{***} + \text{H}^*$ | -0.87 | 0.18 | 0.12 | 0.09 | 0.08 | 0.06 |
| 52 | $\text{CH}_3\text{CH}_2\text{COH}^* + 3* \rightarrow \text{CH}_3\text{CH}_2\text{CO}^{***} + \text{H}^*$ | -0.25 | 0.04 | 0.04 | 0.02 | 0.04 | 0.02 |
| 53 | $\text{CH}_3\text{CH}_2\text{CHO}^* + 3* \rightarrow \text{CH}_3\text{CHCHO}^{***} + \text{H}^*$ | -0.24 | 0.69 | 0.03 | -0.02 | 0.05 | 0.02 |
| 54 | $\text{CH}_3\text{CHCH}_2\text{O}^{***} + * \rightarrow \text{CH}_3\text{CHCHO}^{***} + \text{H}^*$ | -0.67 | -0.06 | 0.01 | -0.02 | 0.01 | -0.01 |
| 55 | $\text{CH}_3\text{CHCHOH}^{**} + 2* \rightarrow \text{CH}_3\text{CHCHO}^{***} + \text{H}^*$ | 0.15 | 0.50 | 0.02 | 0.02 | 0.03 | 0.03 |
| 56 | $\text{CH}_3\text{CH}_2\text{COH}^* + 3* \rightarrow \text{CH}_3\text{CHCOH}^{***} + \text{H}^*$ | -0.28 | 1.07 | 0.00 | -0.15 | 0.02 | -0.08 |
| 57 | $\text{CH}_3\text{CHCHOH}^{**} + 2* \rightarrow \text{CH}_3\text{CHCOH}^{***} + \text{H}^*$ | -0.51 | 0.45 | 0.06 | 0.01 | 0.05 | 0.01 |
| 58 | $\text{CH}_3\text{CH}_2\text{CH}_2\text{O}^* + * \rightarrow \text{CH}_3\text{CH}_2\text{CHO}^* + \text{H}^*$ | -0.63 | 0.02 | -0.09 | 0.00 | -0.06 | 0.00 |
| 59 | $\text{CH}_3\text{CH}_2\text{CHOH}^* + * \rightarrow \text{CH}_3\text{CH}_2\text{CHO}^* + \text{H}^*$ | 0.14 | 0.69 | -0.07 | 0.00 | -0.04 | 0.01 |
| 60 | $\text{CH}_3\text{CH}_2\text{CHOH}^* + * \rightarrow \text{CH}_3\text{CH}_2\text{COH}^* + \text{H}^*$ | -0.48 | 0.28 | 0.01 | 0.02 | 0.01 | 0.02 |
| 61 | $\text{CH}_3\text{CH}_2\text{CH}_2\text{O}^* + 3* \rightarrow \text{CH}_3\text{CHCH}_2\text{O}^{***} + \text{H}^*$ | -0.20 | 0.69 | -0.07 | -0.12 | -0.02 | -0.05 |
| 62 | $\text{CH}_3\text{CHCH}_2\text{OH}^{**} + 2* \rightarrow \text{CH}_3\text{CHCH}_2\text{O}^{***} + \text{H}^*$ | 0.24 | 0.58 | 0.08 | 0.08 | 0.07 | 0.06 |
| 63 | $\text{CH}_3\text{CH}_2\text{CHOH}^* + 2* \rightarrow \text{CH}_3\text{CHCHOH}^{**} + \text{H}^*$ | -0.25 | 0.74 | -0.06 | -0.09 | -0.02 | -0.03 |
| 64 | $\text{CH}_3\text{CHCH}_2\text{OH}^{**} + * \rightarrow \text{CH}_3\text{CHCHOH}^{**} + \text{H}^*$ | -0.58 | 0.51 | 0.07 | -0.14 | 0.05 | -0.09 |
| 65 | $\text{CH}_3\text{CH}_2\text{CH}_2\text{OH}^* + * \rightarrow \text{CH}_3\text{CH}_2\text{CH}_2\text{O}^* + \text{H}^*$ | 0.35 | 0.71 | 0.01 | 0.02 | 0.03 | 0.03 |
| 66 | $\text{CH}_3\text{CH}_2\text{CH}_2\text{OH}^* + * \rightarrow \text{CH}_3\text{CH}_2\text{CHOH}^* + \text{H}^*$ | -0.41 | 0.46 | -0.01 | -0.04 | 0.00 | -0.02 |
| 67 | $\text{CH}_3\text{CH}_2\text{CH}_2\text{OH}^* + 2* \rightarrow \text{CH}_3\text{CHCH}_2\text{OH}^{**} + \text{H}^*$ | -0.09 | 0.78 | -0.14 | -0.16 | -0.07 | -0.08 |
| 68 | $\text{CH}_3\text{CH}_2\text{CH}_2\text{OH}(\text{g}) + * \rightarrow \text{CH}_3\text{CH}_2\text{CH}_2\text{OH}^*$ | 0.66 | N/A | -0.14 | N/A | -0.12 | N/A |
| 69 | $\text{CH}_3\text{CH}_2\text{CHO}(\text{g}) + * \rightarrow \text{CH}_3\text{CH}_2\text{CHO}^*$ | 0.70 | N/A | -0.22 | N/A | -0.16 | N/A |
| 70 | $\text{C}_4\text{H}_8\text{O}_2(\text{dioxane}) + 2* \rightarrow \text{C}_4\text{H}_8\text{O}_2^{**}$ | 1.07 | N/A | -0.30 | N/A | -0.22 | N/A |

3.1 Solvent effects on various elementary reaction steps

Water and 1,4-dioxane are chosen as solvents because they are usually used in experimental studies. The free energies at a temperature of 473 K of various steps are shown in Table 1 with the effects of solvents being shown as corrections to the reaction and activation free energies. Generally, solvents stabilize the adsorption of gas phase species in the range of 0.05 eV to 0.26 eV, and water has a stronger effect than 1,4-dioxane. For example, water stabilizes the adsorption of propionic acid and propionaldehyde adsorption by 0.26 and 0.22 eV, respectively, while the stabilization is 0.20 and 0.16 eV in 1,4-dioxane, respectively. However, solvents have a weaker effect on the reaction and activation free energies for surface reaction steps. Only for a few steps do we observe changes in free energy larger than 0.10 eV as a result of the presence of liquid water. For decarbonylation steps that produce CO, the reaction energies in water are around 0.1 eV more exergonic than in the gas phase as a result of CO adsorption being stabilized in water by 0.15 eV. For the $\text{CH}_3\text{CH}_2\text{COO}$ α -carbon dehydrogenation step in water, the reaction and activation free energies decrease by 0.10 eV and 0.17 eV, respectively. Stabilization is a result of the carboxylate group changing its exposure to the liquid phase during reaction (in the reactant state the carboxylate group points to the surface while in the product state it points at least partially to the liquid phase). For decarboxylation of CH_3CCOO in water, the reaction and activation free energies increase by 0.11 eV and 0.18 eV, respectively. Again, the solvent effect can be understood from the change in exposure of the carboxylate group to the liquid phase during reaction (in the reactant state the carboxylate group points to the liquid phase since the dehydrogenated α -carbon is strongly bound to the surface while in the product state CO_2 species is not partially charged anymore). For almost all other surface reactions, the change in free energy is smaller than 0.10 eV in liquid 1,4-dioxane. The free energies calculated at $\pm 10\%$ of the default COSMO Pt cavity are shown in Table S1 and S2. Overall, the observed trends are very similar to those shown in Table 1. Interestingly, a larger Pt cavity radius leads to a larger solvent effect for adsorption processes and a smaller solvent effect for processes involving a change in exposure of the carboxylate group to the liquid phase. A more detailed discussion of the effects of solvents on the observed kinetics is presented in the following sections.

Table 2 TOFs (s^{-1}) and surface coverage of the most abundant surface intermediates under vapor phase and liquid water and 1,4-dioxane conditions on a Pt (111) surface at a propionic acid partial pressure of 1 bar, CO partial pressure of 0.001 bar and a H_2 partial pressure of 0.1 bar with temperatures ranging from 473 K to 523 K.

| Phase | Temperature (K) | TOF (s ⁻¹) | θ_{H^*} | θ_{CO^*} | θ^* | θ_{Pac} |
|--------------|-----------------|------------------------|----------------|-----------------|------------|----------------|
| Gas | 473 | 1.79×10^{-6} | 0.26 | 0.32 | 0.42 | 0.00 |
| | 498 | 5.92×10^{-6} | 0.26 | 0.27 | 0.47 | 0.00 |
| | 523 | 1.80×10^{-5} | 0.27 | 0.22 | 0.51 | 0.00 |
| water | 473 | 2.27×10^{-6} | 0.04 | 0.49 | 0.07 | 0.40 |
| | 498 | 1.68×10^{-4} | 0.07 | 0.48 | 0.19 | 0.26 |
| | 523 | 2.77×10^{-3} | 0.09 | 0.45 | 0.36 | 0.09 |
| 1, 4-dioxane | 473 | 4.47×10^{-5} | 0.11 | 0.47 | 0.25 | 0.16 |
| | 498 | 3.52×10^{-4} | 0.14 | 0.43 | 0.41 | 0.02 |
| | 523 | 8.93×10^{-4} | 0.16 | 0.37 | 0.47 | 0.00 |

3.2 Microkinetic Modelling

3.2.1 Models and Activity Results

The microkinetic model based on the reaction network shown in Fig. 1 was solved until steady state at temperatures of 473, 498, and 523 K. The gas phase partial pressure was set to 1 bar for propionic acid, 0.001 bar for CO gas, 0.1 bar for hydrogen and zero for all other gas phase molecules, i.e., low conversion conditions. We note that the partial pressures of H₂O and CO₂ have no effect on our results except that they might promote the water-gas shift reaction, which is not explicitly considered in our models. Also, the solvent fugacity of 1,4-dioxane and water was found not to affect our results since the surface coverage of localized water and 1,4-dioxane was found to be small (Table S3 in the SI). In the following, the reported turnover frequency (TOF) corresponds to the rate of consumption of propionic acid per surface Pt atom. Table 2 shows the TOFs and coverages of the most abundant intermediates at different temperatures under both gas phase and liquid phase conditions.

Under gas phase conditions and 473 K, the coverages of CO*, H* and free site are 26%, 32% and 42%, respectively. Surface coverages are not a strong function of temperature, although the CO* coverage decreases somewhat with increasing temperature. In the presence of liquid 1,4-dioxane, CO*, H* and free site remain the dominant surface species; although at 473 K, the propionic acid coverage becomes 16%, somewhat reducing the hydrogen and free site coverage. The surface coverage of CO* is increased to 47% in liquid 1,4-dioxane mainly due to solvent stabilization of CO* as discussed in section 3.1. This effect is even more pronounced in the presence of liquid water. Here, H is not an abundant surface intermediate with a surface coverage less than 10% at all investigated temperatures. In contrast, CO* covers nearly 50% of the surface sites. Due to the strong stabilization effect of water on adsorbed propionic acid, the coverage of propionic acid becomes 40% at 473 K, which leads to a decreasing coverage of free sites (7%).

With increased temperature, the coverage of propionic acid decreases and more free sites become available for surface reactions to take place in water.

Under gas phase conditions, DFT predicts that the reaction has a low TOF of $1.79 \times 10^{-6} \text{ s}^{-1}$ at 473 K on a Pt (111) surface. This TOF increases significantly in liquid 1,4-dioxane with the acceleration increasing with temperature (factor 25 to 50 increase). At 523 K, we predict a TOF in liquid 1,4-dioxane of $8.93 \times 10^{-4} \text{ s}^{-1}$. In contrast, liquid water does not change the TOF significantly at 473 K relative to the gas phase (less than factor 3 increase) because $\text{CH}_3\text{CH}_2\text{COOH}^*$ and CO^* block 89% of the surface sites (the free site coverage is only 7%). However, at higher temperatures in liquid water, the $\text{CH}_3\text{CH}_2\text{COOH}^*$ coverage is significantly reduced, and liquid water starts to accelerate the consumption of propionic acid. For instance, at 523 K the TOF is increased by two orders of magnitude (factor 154) compared to the gas phase, which is even three times larger than that computed in 1,4-dioxane. These results suggest that solvents can significantly affect the reaction kinetics of propionic acid HDO on a Pt (111) surface; however, the selection of an optimal solvent is strongly temperature dependent since solvents affect many processes, some of which accelerate while others decelerate the overall kinetics.

3.2.2 Dominant Pathways

3.2.2.1 Dominant Pathways for the DCN mechanism

There are basically two types of reaction pathways involved in the DCN mechanism as shown in Fig 1a, 2a and 3a: (1) pathways that start with dehydroxylation, $\text{CH}_3\text{CH}_2\text{COOH}^* + 3^* \rightarrow \text{CH}_3\text{CH}_2\text{CO}^{***} + \text{OH}^*$ and followed by either direct decarbonylation or one step of dehydrogenation prior to the decarbonylation, which will be denoted as direct-DCN-path1 and direct-DCN-path2, respectively, and (2) pathways that involve α -carbon dehydrogenation prior to the dehydroxylation step that precedes the decarbonylation, which will be named as indirect-DCN-path. The rates (in s^{-1}) of all elementary reaction steps involved in the DCN mechanism under both gas and liquid phases environments (calculated with default COSMO Pt cavity) are shown in Fig. 1a, 2a and 3a, respectively.

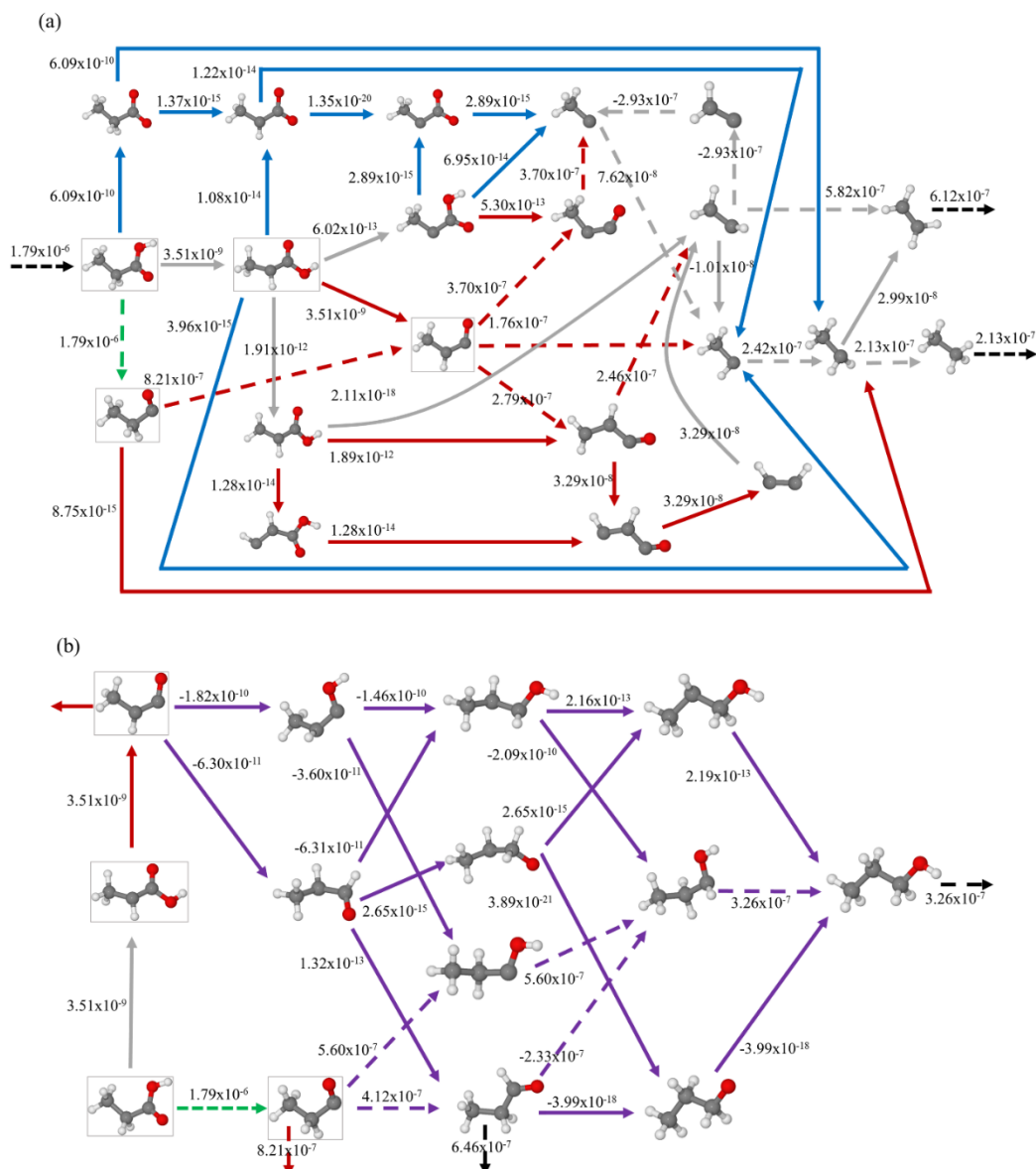


Figure 1. TOFs (s⁻¹) of various elementary steps under vapor phase conditions at a temperature of 473 K, a propionic acid gas phase partial pressure of 1 bar, a CO gas phase partial pressure of 0.001 bar and a hydrogen partial pressure of 0.1 bar. For convenience, black arrows are the adsorption/desorption steps, blue arrows are DCX steps, red arrows are DCN steps, purple steps are steps involved in propanol and propionaldehyde productions, while gray arrows are the steps involved in both DCN and DCX steps and green arrows are steps involved in DCN and propanol and propionaldehyde productions. Dominant pathways are shown in dashed arrows. TOFs (s⁻¹) of reaction steps involved in DCX and DCN are shown in (a) while the TOFs (s⁻¹) for propanol and propionaldehyde production steps are shown in (b).

As shown in Fig. 1a, under vapor phase conditions, the direct-DCN-path2 has a rate of $8.21 \times 10^{-7} \text{ s}^{-1}$ which is more than two orders of magnitude larger than that of the indirect-DCN-path and around 8 orders of magnitude larger than that of the direct-DCN-path1, i.e., the direct-DCN-path2 is the dominant DCN path. According to the rates shown in Fig. 1a, the DCN path

starts with the direct dehydroxylation of adsorbed propionic acid ($\text{CH}_3\text{CH}_2\text{COOH}^* \rightarrow \text{CH}_3\text{CH}_2\text{CO}^{***} + \text{OH}^*$), followed by one step of α -carbon dehydrogenation of $\text{CH}_3\text{CH}_2\text{CO}^{***}$ ($\text{CH}_3\text{CH}_2\text{CO}^{***} \rightarrow \text{CH}_3\text{CHCO}^{**} + \text{H}^*$) forming $\text{CH}_3\text{CHCO}^{**}$, which will go in three possible reaction directions: (1) one step of dehydrogenation of β -carbon prior to the decarbonylation ($\text{CH}_3\text{CHCO}^{**} \rightarrow \text{CH}_2\text{CHCO}^{***} + \text{H}^*$) step followed by hydrogenation of the decarbonylation product $\text{CH}_2\text{CH}^{***}$ to yield CH_2CH_2 , (2) one more dehydrogenation step at the α -carbon of $\text{CH}_3\text{CHCO}^{**}$ ($\text{CH}_3\text{CHCO}^{**} \rightarrow \text{CH}_3\text{CCO}^{***} + \text{H}^*$) followed by decarbonylation of $\text{CH}_3\text{CCO}^{***}$ and hydrogenation/dehydrogenation of the DCN product CH_3C^* to the final product CH_2CH_2 , or (3) decarbonylation of $\text{CH}_3\text{CHCO}^{**}$ to $\text{CH}_3\text{CH}^{**}$ ($\text{CH}_3\text{CHCO}^{**} \rightarrow \text{CH}_3\text{CH}^{**} + \text{CO}^*$) followed by hydrogenation of $\text{CH}_3\text{CH}^{**}$ to the final product CH_3CH_3 . These three reactions happen competitively on the surface with a rate of the same order of magnitude.

In liquid 1,4-dioxane, the rate of the direct-DCN-path2 is increased slightly (~20%) over the gas phase while the rate of the indirect-DCN-path is increased by almost a factor 6. However, the direct-DCN-path2 is still much faster than indirect-DCN-path and direct-DCN-path1, and no matter whether water or dioxane is presented as solvent, the rate of the direct-DCN-path1 is always negligible. Therefore, the dominant pathway of the DCN is not changed by 1,4-dioxane except that the decarbonylation of $\text{CH}_3\text{CHCO}^{**}$ ($\text{CH}_3\text{CHCO}^{**} \rightarrow \text{CH}_3\text{CH}^{**} + \text{CO}^*$), which is the product of the dehydroxylation step of the direct -DCN-path2, is slightly faster than the two competitive dehydrogenation steps ($\text{CH}_3\text{CHCO}^{**} \rightarrow \text{CH}_2\text{CHCO}^{***} + \text{H}^*$, $\text{CH}_3\text{CHCO}^{**} \rightarrow \text{CH}_3\text{CCO}^{***} + \text{H}^*$). Interestingly, the rate of the direct-DCN-path2 is decreased from $8.21 \times 10^{-7} \text{ s}^{-1}$ in the gas phase to $2.82 \times 10^{-8} \text{ s}^{-1}$ when water is present as solvent, while the rate of the indirect-DCN-path is increased to $6.25 \times 10^{-9} \text{ s}^{-1}$, i.e., it becomes nearly competitive to the direct-DCN-path2. So, the dominant pathway of the DCN remains unchanged by the presence of liquid water, except that the decarbonylation of $\text{CH}_3\text{CHCO}^{**}$ to $\text{CH}_3\text{CH}^{**}$ ($\text{CH}_3\text{CHCO}^{**} \rightarrow \text{CH}_3\text{CH}^{**} + \text{CO}^*$) is faster than $\text{CH}_3\text{CHCO}^{**} \rightarrow \text{CH}_2\text{CHCO}^{***} + \text{H}^*$ and $\text{CH}_3\text{CHCO}^{**} \rightarrow \text{CH}_3\text{CCO}^{***} + \text{H}^*$. Surprisingly, even though the TOF is increased in liquid, the rate of the DCN pathways does not increase significantly and even becomes smaller in water. This is because propanol and propionaldehyde production dominate the HDO of propionic acid in the liquid phase, and around 98% of the adsorbed propionic acid is hydrogenated to propanol and propionaldehyde, which will be further discussed in the following section 3.2.2.2.

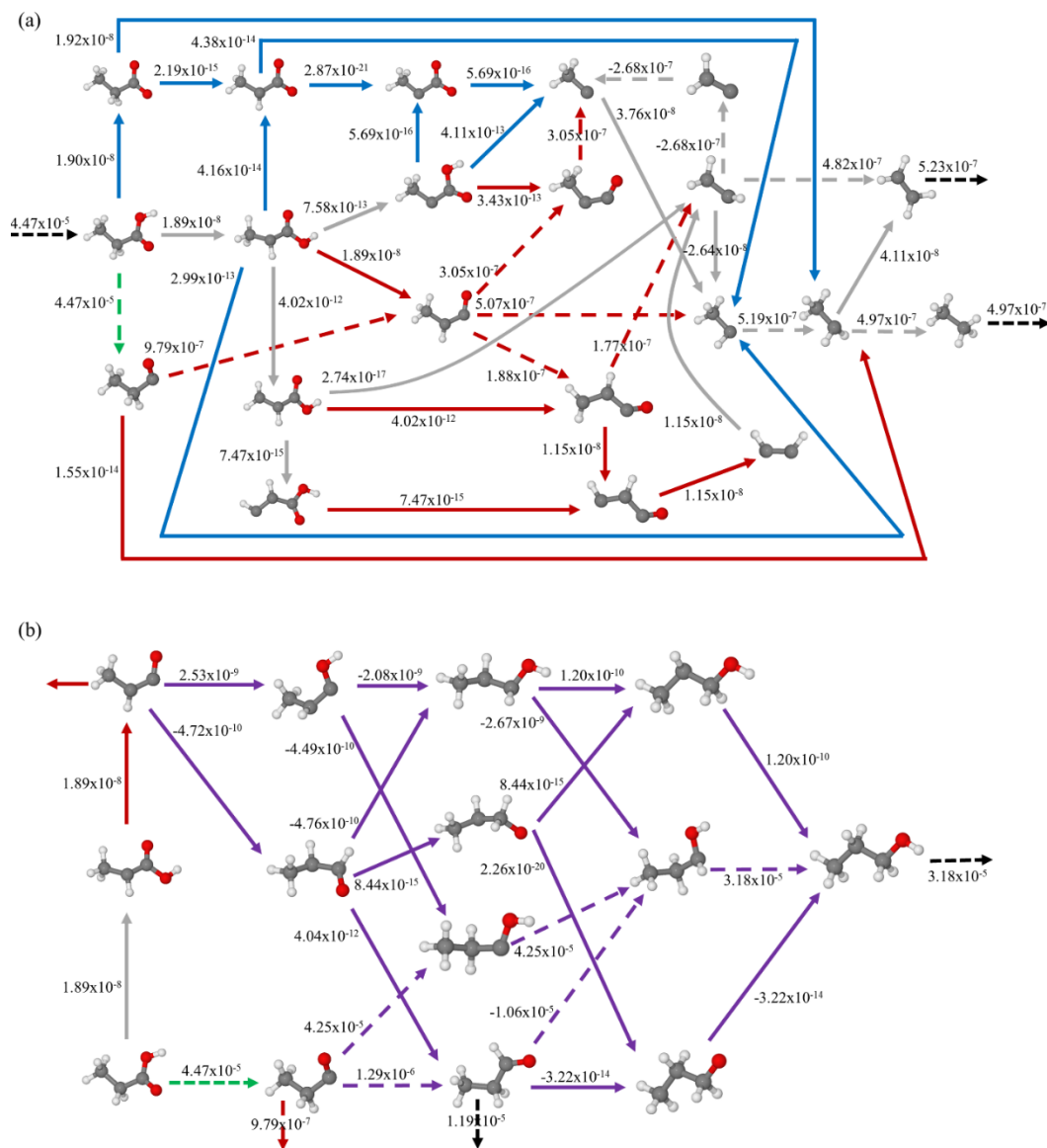


Figure 2 TOFs (s⁻¹) of various elementary steps in the presence of liquid 1,4-dioxane at a temperature of 473 K, a propionic acid gas phase partial pressure of 1 bar, a CO gas phase partial pressure of 0.001 bar and a hydrogen partial pressure of 0.1 bar. For convenience, black arrows are the adsorption/desorption steps, blue arrows are DCX steps, red arrows are DCN steps, purple steps are steps involved in propanol and propionaldehyde productions, while gray arrows are the steps involved in both DCN and DCX steps and green arrows are steps involved in DCN and propanol and propionaldehyde productions. Dominant pathways are shown in dashed arrows. TOFs (s⁻¹) of reaction steps involved in DCX and DCN are shown in (a) while the TOFs (s⁻¹) for propanol and propionaldehyde production steps are shown in (b).

Overall, under both vapor and liquid phase conditions, the dominant pathway of the DCN is the direct-DCN-path2, which first involves direct dehydroxylation of propionic acid, followed by α -carbon dehydrogenation, and then dependent on the reaction environment, either direct

decarbonylation or dehydrogenation of the α - or β -carbon prior to decarbonylation. Finally, hydrogenation of the decarbonylation product will occur to finish the DCN path.

3.2.2.2 Dominant Pathways for Propanol and Propionaldehyde Production

As shown in Fig. 1b, 2b and 3b, we mainly considered three possible pathways for propanol production: (1) direct dehydroxylation of the adsorbed $\text{CH}_3\text{CH}_2\text{COOH}^*$, followed by hydrogenation of the carbonyl group of $\text{CH}_3\text{CH}_2\text{CO}^{***}$ to form propanol, which will be referred to as direct-propanol-path, (2) a dehydrogenation step (either α - or β -carbon) taking place prior to dehydroxylation, followed by a couple of hydrogenation steps after dehydroxylation forming propanol, which will be denoted as the indirect-propanol-path, and (3) hydrogenation of the produced propionaldehyde to propanol. We intentionally neglect this third pathway in our discussion here since it is much slower than the other two pathways according to Fig. 1b, 2b and 3b. Similarly, we also considered three possible pathways for propionaldehyde production: (1) direct dehydroxylation of the adsorbed $\text{CH}_3\text{CH}_2\text{COOH}$ forming a single hydrogen deficient aldehyde ($\text{CH}_3\text{CH}_2\text{CO}^{***}$), followed by one hydrogenation step to form propionaldehyde on the surface, which will be referred as direct-aldehyde-path, (2) dehydrogenation of one hydrogen deficient propanol that is produced in the direct-propanol-path to form propionaldehyde, i.e., $\text{CH}_3\text{CH}_2\text{COOH}^* \rightarrow \text{CH}_3\text{CH}_2\text{CO}^{***} \rightarrow \text{CH}_3\text{CH}_2\text{COH}^* \rightarrow \text{CH}_3\text{CH}_2\text{CHOH}^* \rightarrow \text{CH}_3\text{CH}_2\text{CHO}^*$, which will be called indirect-aldehyde-path, and (3) dehydrogenation prior to dehydroxylation, followed by hydrogenation to propionaldehyde, which will also be neglected as it is much slower than the other two pathways as shown in Fig. 1b, 2b and 3b.

Under vapor phase conditions, the dominant pathways for propanol and propionaldehyde production are both direct formation pathways, which start with dehydroxylation of the adsorbed propionic acid ($\text{CH}_3\text{CH}_2\text{COOH}^* \rightarrow \text{CH}_3\text{CH}_2\text{CO}^{***} + \text{OH}^*$). About 46% of the produced $\text{CH}_3\text{CH}_2\text{CO}^{***}$ follows a decarbonylation mechanism while the rest goes into two competing directions: (1) one carbon atom hydrogenation step to produce propionaldehyde on the surface and (2) hydrogenation of the oxygen atom of the carbonyl group of $\text{CH}_3\text{CH}_2\text{CO}^{***}$ forming a propanol-like intermediate $\text{CH}_3\text{CH}_2\text{COH}^*$ on the surface. The rates for these processes are $4.12 \times 10^{-7} \text{ s}^{-1}$ and $5.60 \times 10^{-8} \text{ s}^{-1}$, respectively. $\text{CH}_3\text{CH}_2\text{COH}^*$ can be further hydrogenated to $\text{CH}_3\text{CH}_2\text{CHOH}^*$. About 33% of $\text{CH}_3\text{CH}_2\text{CHOH}^*$ is further hydrogenated to propanol while about 67% of $\text{CH}_3\text{CH}_2\text{CHOH}^*$ is dehydrogenated to propionaldehyde ($\text{CH}_3\text{CH}_2\text{CHO}^*$). As shown in Table 3, the overall selectivity of the DCN, propanol and propionaldehyde production pathways

in the vapor phase are predicted to be 46%, 18% and 36%, respectively, indicating that propanol and propionaldehyde can be produced during the HDO of propionic acid over Pt (111) surface. This observation agrees very well with our preliminary experimental results.

In both liquid water and 1,4-dioxane, the dominant pathway for propanol production is always the direct-propanol-path, while that for propionaldehyde is changed from the direct pathway to the indirect pathway. As shown in Fig. 2b and 3b, the first step for propanol and propionaldehyde production is still the direct dehydroxylation of adsorbed $\text{CH}_3\text{CH}_2\text{COOH}^*$ forming $\text{CH}_3\text{CH}_2\text{CO}^{***}$ on the surface. In the following, however, hydrogenation of $\text{CH}_3\text{CH}_2\text{CO}^{***}$ to propionaldehyde can no longer compete with hydrogenation of $\text{CH}_3\text{CH}_2\text{CO}^{***}$ to $\text{CH}_3\text{CH}_2\text{COH}^*$. In liquid water, the rates of these processes are $5.73 \times 10^{-9} \text{ s}^{-1}$ and $2.22 \times 10^{-6} \text{ s}^{-1}$, respectively, while they are $1.29 \times 10^{-6} \text{ s}^{-1}$ and $4.25 \times 10^{-5} \text{ s}^{-1}$, respectively, in 1,4-dioxane. Then, $\text{CH}_3\text{CH}_2\text{COH}^*$ will go through one hydrogenation step to form $\text{CH}_3\text{CH}_2\text{CHOH}^*$, which will partly be dehydrogenated to propionaldehyde (from 23% to 30% depending on the solvent and the cavity of Pt as demonstrated by the selectivity shown in Table 3) with the remainder being hydrogenated to propanol. What's more, unlike in the gas phase where 46% of the $\text{CH}_3\text{CH}_2\text{CO}^{***}$ species is decarbonylated, almost all the produced $\text{CH}_3\text{CH}_2\text{CO}^{***}$ (around 98% in both liquid water and 1,4-dioxane) will be hydrogenated to $\text{CH}_3\text{CH}_2\text{COH}^*$. Due to this change in dominant pathway, the selectivity of propanol increased dramatically in the condensed phase from 18% to around 70-75%, while the selectivity of DCN products dramatically dropped from 46% to around 2%. The selectivity of propionaldehyde is less sensitive to the reaction environment and 23 to 36% of the reaction flux goes towards propionaldehyde.

Table 3 Product selectivity under gas and liquid phase conditions at a temperature of 473 K, a propionic acid gas phase partial pressure of 1 bar, a CO gas phase partial pressure of 0.001 bar and a hydrogen partial pressure of 0.1 bar. Results from solvation calculations with $\pm 10\%$ of default COMSO Pt cavity radius are also shown for water and 1,4-dioxane. N/A denotes that the value is smaller than 0.01.

| | gas | water (default) | water (+10%) | water (-10%) | 1, 4-dioxane (default) | 1, 4-dioxane (+10%) | 1, 4-dioxane (-10%) |
|------------------------|------|--------------------|-----------------|-----------------|---------------------------|------------------------|------------------------|
| S_{DCX} | N/A | N/A | 0.01 | 0.01 | N/A | N/A | N/A |
| S_{DCN} | 0.46 | 0.02 | 0.01 | 0.01 | 0.02 | 0.02 | 0.02 |
| S_{propanol} | 0.18 | 0.74 | 0.75 | 0.69 | 0.71 | 0.70 | 0.68 |
| $S_{\text{propional}}$ | 0.36 | 0.24 | 0.23 | 0.30 | 0.27 | 0.28 | 0.30 |

In summary, while the dominant pathway for propanol production remains unchanged in both gas and liquid phase environments, the dominant pathway for propionaldehyde production changed from a direct formation pathway to an indirect pathway. What's more, the solvent greatly

promotes the rate of propanol production, which leads to a dramatic increase in the selectivity towards propanol and a decrease in selectivity of DCN products.

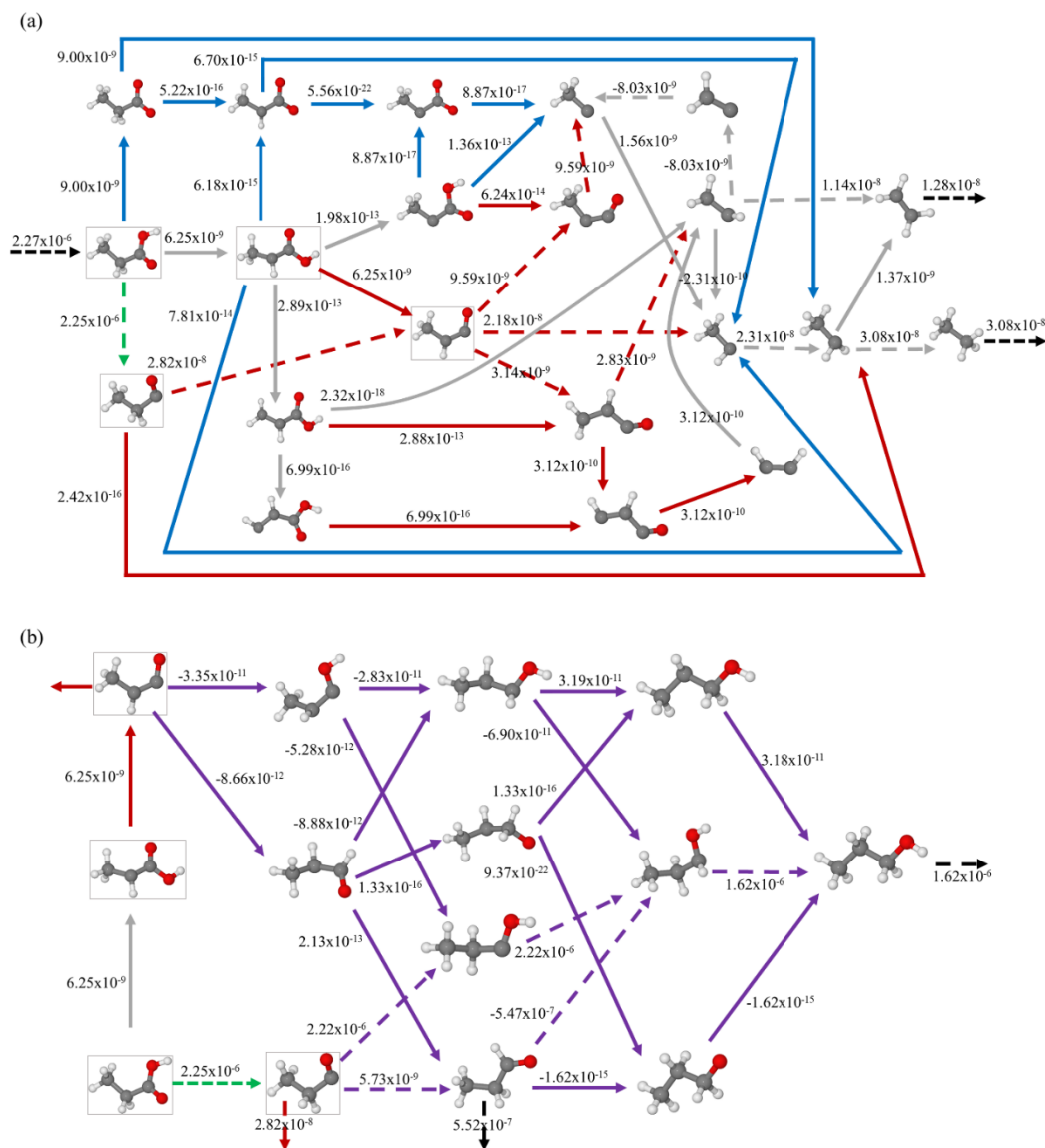


Figure 3 TOFs (s⁻¹) of various elementary steps in the presence of liquid water at a temperature of 473 K, a propionic acid gas phase partial pressure of 1 bar, a CO gas phase partial pressure of 0.001 bar and a hydrogen partial pressure of 0.1 bar. For convenience, black arrows are the adsorption/desorption steps, blue arrows are DCX steps, red arrows are DCN steps, purple steps are steps involved in propanol and propionaldehyde productions, while gray arrows are the steps involved in both DCN and DCX steps and green arrows are steps involved in DCN and propanol and propionaldehyde productions. Dominant pathways are shown in dashed arrows. TOFs (s⁻¹) of reaction steps involved in DCX and DCN are shown in (a) while the TOFs (s⁻¹) for propanol and propionaldehyde production steps are shown in (b).

3.2.2.3 Dominant Pathways for the DCX

There are at least five potentially relevant reaction pathways identified from our earlier research on Pd and Ru catalysts: (1) dehydrogenation of the carboxyl group in adsorbed propionic acid prior to decarboxylation followed by hydrogenation steps to the final products ethane or ethene ($\text{CH}_3\text{CH}_2\text{COOH}^* \rightarrow \text{CH}_3\text{CH}_2\text{COO}^{**} \rightarrow \text{CH}_3\text{CH}_2^* \rightarrow \text{CH}_3\text{CH}_3^*$), (2) same carboxyl group dehydrogenation as in pathway 1 followed by α -carbon dehydrogenation before decarboxylation and hydrogenation of the decarboxylation product to ethane ($\text{CH}_3\text{CH}_2\text{COOH}^* \rightarrow \text{CH}_3\text{CH}_2\text{COO}^* \rightarrow \text{CH}_3\text{CHCOO}^{***} \rightarrow \text{CH}_3\text{CH}^{**} \rightarrow \text{CH}_3\text{CH}_2^* \rightarrow \text{CH}_3\text{CH}_3^*$), (3) this pathway is almost the same as pathway 2 except that the α -carbon is fully dehydrogenated prior to decarboxylation ($\text{CH}_3\text{CH}_2\text{COOH}^* \rightarrow \text{CH}_3\text{CH}_2\text{COO}^{**} \rightarrow \text{CH}_3\text{CHCOO}^{***} \rightarrow \text{CH}_3\text{CCOO}^{***} \rightarrow \text{CH}_3\text{C}^* \rightarrow \text{CH}_3\text{CH}_2^* \rightarrow \text{CH}_3\text{CH}_3^*$), (4) in this pathway, one or two α -carbon dehydrogenation steps occur before dehydrogenation of the carboxyl group and decarboxylation ($\text{CH}_3\text{CH}_2\text{COOH}^* \rightarrow \text{CH}_3\text{CHCOOH}^{**} \rightarrow \text{CH}_3\text{CCOOH}^{***} \rightarrow \text{CH}_3\text{CCOO}^{***} \rightarrow \text{CH}_3\text{C}^* \rightarrow \text{CH}_3\text{CH}_2^* \rightarrow \text{CH}_3\text{CH}_3^*$), (5) both α - and β -carbon dehydrogenation prior to dehydrogenation of the carboxyl group and decarboxylation.

No matter the reaction environment (vapor or liquid water or 1,4-dioxane), the dominant pathway for the DCX is always pathway 1. The rate of the DCX is very small and at least 3 orders of magnitude smaller than the DCN, propanol, and propionaldehyde production pathways, which agrees well with our preliminary experimental results. In condensed water and 1,4-dioxane, the DCX rate increases by at least one order of magnitude relative to the vapor phase but overall remains much smaller than the rate for propanol and propionaldehyde production. Thus, the selectivity towards DCX remains negligible in all reaction environments. Our prediction that the DCX pathway is not favored during the HDO of propionic acid, but that the rate increases in condensed phases agrees very well with previous studies on the HDO of propionic and acetic acid on other metal surfaces[10, 14, 20, 22, 41].

3.2.3 Sensitivity Analysis

To carry out a sensitivity analysis of our results, we computed Campbell's degree of kinetic rate control, DRC_i , and selectivity control, DSC_i , where i can be either a transition state or stable adsorbed intermediate[42, 43]. This enables discovery of the rate- and selectivity controlling steps and surface intermediates in the HDO of propionic acid over Pt (111). The degree of rate control and selectivity control can be calculated using the following equations.

$$\text{DRC}_i = \left(\frac{\partial \ln r}{\partial \frac{-G_i^0}{RT}} \right)_{G_{j \neq i}^0} \quad (16)$$

$$\text{DSC}_i = \left(\frac{\partial(\ln rP/rR)}{\partial \frac{-G_i^0}{RT}} \right)_{G_{j \neq i}^0} = \left(\frac{\partial(\ln rP)}{\partial \frac{-G_i^0}{RT}} \right)_{G_{j \neq i}^0} - \left(\frac{\partial(\ln rR)}{\partial \frac{-G_i^0}{RT}} \right)_{G_{j \neq i}^0} = \text{DRC}_{i,P} - \text{DRC}_{i,R} \quad (17)$$

where the partial derivative is taken holding constant the standard-state free energy of all other species G_j^0 (intermediates, transition states, reactants, and products). The value of DRC_i describes the relative increase in net rate due to the (differential) stabilization of the standard-state free energy for species i , holding all the other species' energies constant. $\text{DRC}_{i,P}$ and $\text{DRC}_{i,R}$ are the degrees of rate control of species i for the rates of making product P and consuming reactant R , respectively. The value of DSC_i describes the relative increase in net selectivity to product P from reactant R due to the (differential) stabilization of the standard-state free energy for species i (either a transition state or stable adsorbed intermediate state), holding all other species' energies constant.

3.2.3.1 Degrees of Rate Control

As shown in Table 4, reaction step 1 ($\text{CH}_3\text{CH}_2\text{COOH}^* + 3^* \rightarrow \text{CH}_3\text{CH}_2\text{CO}^{***} + \text{OH}^*$) solely controls the rate of the reaction (the rate of consumption of propionic acid) under both vapor and liquid phase conditions. The C-OH bond scission has also previously been identified as the rate controlling step in the HDO of propionic acid over Pd (111) and Ru (0001). Similarly, Olcay et al. and Pallassana and Neurock suggested that C-OH bond cleavage is rate controlling in the HDO of acetic acid on Pt (111), Pd (111) and Rh (111) surfaces[20, 44].

Table 4 Degrees of rate control for various steps under gas and liquid phase conditions at a temperature of 473 K, a propionic acid partial pressure of 1 bar, a CO partial pressure of 0.001 bar and a hydrogen partial pressure of 0.1 bar. Results from solvation calculations with $\pm 10\%$ of default COMSO Pt cavity radius are also shown for water and 1,4-dioxane. N/A denotes that the value is smaller than 0.01.

| | gas | water (default) | water (+10%) | water (-10%) | 1, 4-dioxane (default) | 1, 4-dioxane (+10%) | 1, 4-dioxane (-10%) |
|---------|------|--------------------|-----------------|-----------------|---------------------------|------------------------|------------------------|
| Step 1 | 0.96 | 0.96 | 0.95 | 0.96 | 0.96 | 0.96 | 0.96 |
| Step 4 | N/A | -0.05 | -0.10 | -0.01 | -0.03 | -0.03 | -0.01 |
| Step 8 | N/A | -0.02 | -0.04 | -0.01 | N/A | N/A | N/A |
| Step 25 | N/A | 0.06 | 0.12 | 0.03 | 0.02 | 0.02 | 0.01 |

The degrees of thermodynamic rate control of the three most abundant surface intermediates H^* , CO^* and $\text{CH}_3\text{CH}_2\text{COOH}^*$ are listed in Table 5. In the gas phase, the values of

the degrees of thermodynamic rate control for CO* and CH₃CH₂COOH* are 1.84 and 0.96, respectively, demonstrating that stabilizing the adsorption of CO* and CH₃CH₂COOH* can increase the rate of the reaction. In the case of CO*, this observation can be explained by the lateral interactions of CO* with other adsorbates. In contrast, H* has a large negative value of the degree of rate control (-3.04), which indicates that destabilizing the adsorption of H* and creating more free sites for the rate controlling reaction step 1 facilitates the HDO of propionic acid over Pt (111). In the condensed phase, the thermodynamic degrees of rate control change significantly. In liquid water, the H* coverage is small, and a small positive degree of thermodynamic rate control is observed. Also, the CO* and CH₃CH₂COOH* coverages are high such that negative degrees of thermodynamic rate control are computed. Somewhat similarly, in condensed 1,4-dioxane, both H* and CO* have negative degrees of thermodynamic rate control due to the significant surface coverage of these species while CH₃CH₂COOH* has a small positive degree of rate control that is sensitive to the Pt cavity radius in the solvation calculations, given the small but significant propionic acid coverage on the surface.

Table 5 Degrees of thermodynamic rate control for H*, CO* and CH₃CH₂COOH* (the most abundant surface species) under gas and liquid phase conditions at a temperature of 473 K, a propionic acid partial pressure of 1 bar, a CO partial pressure of 0.001 bar and a hydrogen partial pressure of 0.1 bar. Results from solvation calculations with $\pm 10\%$ of default COMSO Pt cavity radius are also shown for water and 1,4-dioxane.

| Surface species | gas | water (default) | water (+10%) | water (-10%) | 1, 4-dioxane (default) | 1, 4-dioxane (+10%) | 1, 4-dioxane (-10%) |
|---------------------------------------|-------|--------------------|-----------------|-----------------|---------------------------|------------------------|------------------------|
| H* | -3.04 | 0.11 | 0.09 | 0.08 | -0.63 | -0.35 | -0.21 |
| CO* | 1.84 | -3.16 | -3.28 | -3.34 | -2.21 | -2.40 | -2.61 |
| CH ₃ CH ₂ COOH* | 0.96 | -0.84 | -1.02 | -0.96 | 0.18 | -0.05 | -0.12 |

3.2.3.2 Degrees of Selectivity Control

The degrees of selectivity control of various key reaction steps for DCX, DCN, propanol, and propionaldehyde production are shown in Table 6, 7, 8 and 9, respectively, and corresponding degrees of selectivity control of various key surface intermediates are shown in Table S5, S6, S7, S8, respectively. Results shown in Table 6 indicate that the selectivity to the DCX path is solely determined by step 1 (CH₃CH₂COOH* + 3* \rightarrow CH₃CH₂CO*** + OH*), i.e., deceleration of the dehydroxylation step increases the selectivity towards DCX most in all reaction environments. From the results of the degrees of thermodynamic selectivity control shown in Table S5, CH₃CH₂COO**, CH₃CH₂COOH*, H* and CO* are the key surface intermediates that have an

apparent effect on the DCX path selectivity. Generally, stabilization of the adsorption of $\text{CH}_3\text{CH}_2\text{CO}^{**}$, which is the key species in the DCX path, can increase the DCX path selectivity. For the other three species, the effect varies dependent on the reaction environment. For instance, stabilization of the CO^* adsorption in gas phase will decrease the DCX path selectivity, while in liquid phase, it will increase the selectivity towards the DCX path.

Table 6 Degrees of selectivity control for various key reaction steps that have impact on DCX path under gas and liquid phase conditions at a temperature of 473 K, a propionic acid partial pressure of 1 bar, a CO partial pressure of 0.001 bar and a hydrogen partial pressure of 0.1 bar. Results from solvation calculations with $\pm 10\%$ of the default COMSO Pt cavity radius are also shown for water and 1,4-dioxane. N/A denotes that the value is smaller than 0.01.

| | Step 1 | Step 5 |
|-----------------------|--------|--------|
| Gas | -0.965 | -0.002 |
| Water (default) | -0.957 | -0.004 |
| Water (+10%) | -0.948 | -0.010 |
| Water (-10%) | -0.957 | 0.002 |
| 1,4-dioxane (default) | -0.973 | 0.013 |
| 1,4-dioxane (+10%) | -0.963 | -0.002 |
| 1,4-dioxane (-10%) | -0.937 | -0.001 |

For DCN products, under gas phase conditions, stabilizing the transition state of reaction step 4 ($\text{CH}_3\text{CH}_2\text{CO}^{***} \rightarrow \text{CH}_3\text{CHCO}^{**} + \text{H}^*$), which competes with steps that lead to propanol and propionaldehyde production, increases the selectivity most. Similarly, destabilizing the transition states for propanol and propionaldehyde formation (reaction step 51, 59 and 66) increases the selectivity towards DCN products. In liquid phase, the reaction flux through step 51 (direct-aldehyde-path) becomes small, so this transition state has a negligible effect on selectivity. In contrast, the propanol and propionaldehyde formation steps (steps 59 and 66) have an even more negative selectivity control towards DCN products in condensed phase. Also, stabilizing the transition state of step 4 continues to increase the selectivity towards DCN in liquid phase. This effect is even more pronounced in liquid 1,4-dioxane. Finally, steps 1 ($\text{CH}_3\text{CH}_2\text{COOH}^* + 3^* \rightarrow \text{CH}_3\text{CH}_2\text{CO}^{***} + \text{OH}^*$), 5 ($\text{CH}_3\text{CHCOOH}^{**} + ^* \rightarrow \text{CH}_3\text{CHCO}^{**} + \text{OH}^*$), and 8 ($\text{CH}_3\text{CHCO}^{**} + ^* \rightarrow \text{CH}_3\text{CH}^{**} + \text{CO}^*$) also affect the selectivity to DCN products somewhat in liquid water. The origin for the selectivity control of these steps is that the indirect-DCN-path (which involves dehydrogenation steps) becomes competitive against the direct-DCN-path in water. As shown in Table S6, stabilizing the adsorption of H^* , $\text{CH}_3\text{CH}_2\text{CO}^{***}$ and $\text{CH}_3\text{CHCO}^{**}$ will increase the selectivity towards the DCN path, while stabilizing the adsorption of those alcohol and aldehyde like intermediates ($\text{CH}_3\text{CH}_2\text{CHOH}^*$, $\text{CH}_3\text{CH}_2\text{CH}_2\text{OH}^*$ and $\text{CH}_3\text{CH}_2\text{CHO}^*$) will decrease the

DCN path selectivity since it will promote the propanol and propionaldehyde production. The effect of CO adsorption on the selectivity varies depending on the reaction environment and the Pt cavity used in the solvent calculations such that we are unable to determine it reliably.

Table 7 Degrees of selectivity control for various key reaction steps that have impact on the DCN path under gas and liquid phase conditions at a temperature of 473 K, a propionic acid partial pressure of 1 bar, a CO partial pressure of 0.001 bar and a hydrogen partial pressure of 0.1 bar. Results from solvation calculations with $\pm 10\%$ of default COMSO Pt cavity radius are also shown for water and 1,4-dioxane. N/A denotes that the value is smaller than 0.01.

| | Step 1 | Step 4 | Step 5 | Step 8 | Step 51 | Step 59 | Step 66 |
|-----------------------|--------|--------|--------|--------|---------|---------|---------|
| Gas | N/A | 0.49 | N/A | 0.01 | -0.23 | -0.13 | -0.18 |
| Water (default) | -0.10 | 0.46 | 0.10 | 0.24 | N/A | -0.21 | -0.62 |
| Water (+10%) | -0.43 | 0.21 | 0.44 | 0.24 | N/A | -0.12 | -0.39 |
| Water (-10%) | -0.22 | 0.20 | 0.23 | 0.36 | N/A | -0.22 | -0.50 |
| 1,4-dioxane (default) | -0.02 | 0.75 | 0.02 | 0.09 | -0.03 | -0.23 | -0.67 |
| 1,4-dioxane (+10%) | -0.02 | 0.76 | 0.02 | 0.09 | -0.02 | -0.25 | -0.64 |
| 1,4-dioxane (-10%) | -0.02 | 0.66 | 0.02 | 0.16 | -0.02 | -0.27 | -0.64 |

Next, for propanol production, Table 8 summarizes the degrees of selectivity control. Stabilizing reaction step 66 ($\text{CH}_3\text{CH}_2\text{CH}_2\text{OH}^* + * \rightarrow \text{CH}_3\text{CH}_2\text{CHOH}^* + \text{H}^*$) and decelerating step 59 ($\text{CH}_3\text{CH}_2\text{CHOH}^* + * \rightarrow \text{CH}_3\text{CH}_2\text{CHO}^* + \text{H}^*$) leads to increased propanol production in all reaction environments. Step 66 facilitates direct propanol production and step 59 determines the relative reaction flux going towards propionaldehyde versus propanol. In the vapor phase, decelerating steps 4 and step 51 also increases the selectivity towards propanol. Step 4 is a key reaction step to produce DCN products while step 51 is instrumental for propionaldehyde production. The stability of these transition states plays only a minor role in condensed phases where the main reaction flux goes to propanol production. Table S7 shows the thermodynamic selectivity control of various key species on propanol production. In the gas phase, stabilization of H^* adsorption changes the selectivity towards alcohol production, while it has a much smaller effect in the condensed phase. In contrast, stabilization of CO^* decreases the propanol selectivity in vapor phase, while it increases the selectivity towards alcohols in condensed phase. Stabilization of key intermediates in the DCN and aldehyde mechanism, $\text{CH}_3\text{CH}_2\text{CO}^{***}$ and $\text{CH}_3\text{CH}_2\text{CHO}^*$, decrease the selectivity towards propanol in the vapor phase. Given that in condensed phase the decarbonylation and aldehyde production is less dominant, these species do not display a selectivity control in condensed phases. Also, stabilizing adsorbed propanol, $\text{CH}_3\text{CH}_2\text{CH}_2\text{OH}^*$, increases the selectivity towards propanol production in all reaction environments as it increases the reaction flux for the hydrogenation of $\text{CH}_3\text{CH}_2\text{CHOH}^*$ towards $\text{CH}_3\text{CH}_2\text{CH}_2\text{OH}^*$.

Table 8 Degrees of selectivity control for various key reaction steps that have impact on the propanol and the propionaldehyde production path under gas and liquid phase conditions at a temperature of 473 K, a propionic acid partial pressure of 1 bar, a CO partial pressure of 0.001 bar and a hydrogen partial pressure of 0.1 bar. Results from solvation calculations with $\pm 10\%$ of default COMSO Pt cavity radius are also shown for water and 1,4-dioxane. N/A denotes that the value is smaller than 0.01. The values in front of the brackets and the values in the brackets corresponding to the degrees of selectivity control for the propanol and the propionaldehyde production path, respectively.

| | Step 4 | Step 51 | Step 59 | Step 66 |
|------------------------|---------------|--------------|--------------|--------------|
| Gas | -0.41 [-0.41] | -0.23 [0.39] | -0.13 [0.22] | 0.79 [-0.18] |
| Water (default) | -0.01 [-0.01] | N/A [0.01] | -0.24 [0.72] | 0.25 [-0.71] |
| Water (+10%) | N/A [N/A] | N/A [N/A] | -0.22 [0.74] | 0.23 [-0.73] |
| Water (-10%) | N/A [N/A] | N/A [N/A] | -0.30 [0.67] | 0.30 [-0.67] |
| 1, 4-dioxane (default) | -0.02 [-0.02] | -0.03 [0.08] | -0.23 [0.62] | 0.28 [-0.68] |
| 1, 4-dioxane (+10%) | -0.02 [-0.02] | -0.02 [0.06] | -0.27 [0.63] | 0.30 [-0.67] |
| 1, 4-dioxane (-10%) | -0.01 [-0.01] | -0.02 [0.04] | -0.28 [0.64] | 0.31 [-0.66] |

Finally, for propionaldehyde production, Table 8 summarizes the degrees of selectivity control. Again, step 59 and 66 are the key rate controlling steps in all reaction environments determining the relative reaction flux going towards propionaldehyde versus propanol. In the vapor phase, where DCN products are also produced, decelerating step 4 ($\text{CH}_3\text{CH}_2\text{CO}^{***} \rightarrow \text{CH}_3\text{CHCO}^{**} + \text{H}^*$) and accelerating the direct aldehyde production step 51 ($\text{CH}_3\text{CH}_2\text{CHO}^* + 3^* \rightarrow \text{CH}_3\text{CH}_2\text{CO}^{***} + \text{H}^*$) also favors production of propionaldehyde. For the surface intermediates that have a significant effect on propionaldehyde selectivity, shown in Table S8, the stability of adsorbed H^* , CO^* , $\text{CH}_3\text{CH}_2\text{CHOH}^*$ and $\text{CH}_3\text{CH}_2\text{CH}_2\text{OH}^*$ are most relevant. Stabilizing H^* adsorption increases the selectivity to propionaldehyde in vapor phase while it has practically no effect in the condensed phase. Stabilizing CO^* reduces the selectivity in the vapor phase while it increases it in liquid water and 1,4-dioxane. Next, stabilizing $\text{CH}_3\text{CH}_2\text{CHOH}^*$ increases the selectivity in all environments, while stabilizing $\text{CH}_3\text{CH}_2\text{CH}_2\text{OH}^*$ decreases the selectivity in all environments, given that these species determine the relative reaction flux going towards alcohol and aldehyde.

3.2.4 Apparent Activation Barrier & Reaction Orders

In order to understand the temperature dependence of the rate of the reaction, apparent activation barriers (E_a) have been calculated using the following equation with a temperature range from 473K to 523K in all reaction environments.

$$E_a = k_B T^2 \left(\frac{d \ln(r_{OF})}{dT} \right)_{P,T} \quad (18)$$

To gain insights into the pressure dependence of the HDO of propionic acid on Pt (111) surface, reaction orders of H_2 and propionic acid have also been calculated using,

$$\alpha_i = \left(\frac{d \ln(\text{TOF})}{d \ln(P_i)} \right)_{T, P_{j \neq i}} \quad (19)$$

Figure 4a illustrates the reaction order with respect to H₂ in the vapor phase (-1.08), liquid 1,4-dioxane (-0.21) and liquid water (0.04). These reaction orders correlate (as expected) very well with the degrees of thermodynamic rate control of H* in the different reaction environments (see Table 5). Similarly, the reaction orders of propionic acid shown in Figure 4b, 1.00 in the vapor phase, 0.15 in 1,4-dioxane, and -0.44 in liquid water, correlate with the degree of thermodynamic rate control of adsorbed propionic acid. While in the vapor phase the propionic acid coverage is very low, the coverage increases in condensed phase with a high coverage in liquid water, where adsorbed propionic acid blocks active sites for reaction. Figure 5 illustrates the change in propionic acid reaction order with temperature in liquid water. With increasing temperature, the surface coverage of propionic acid decreases and thus, the reaction order increases until it reaches close to one at 573 K.

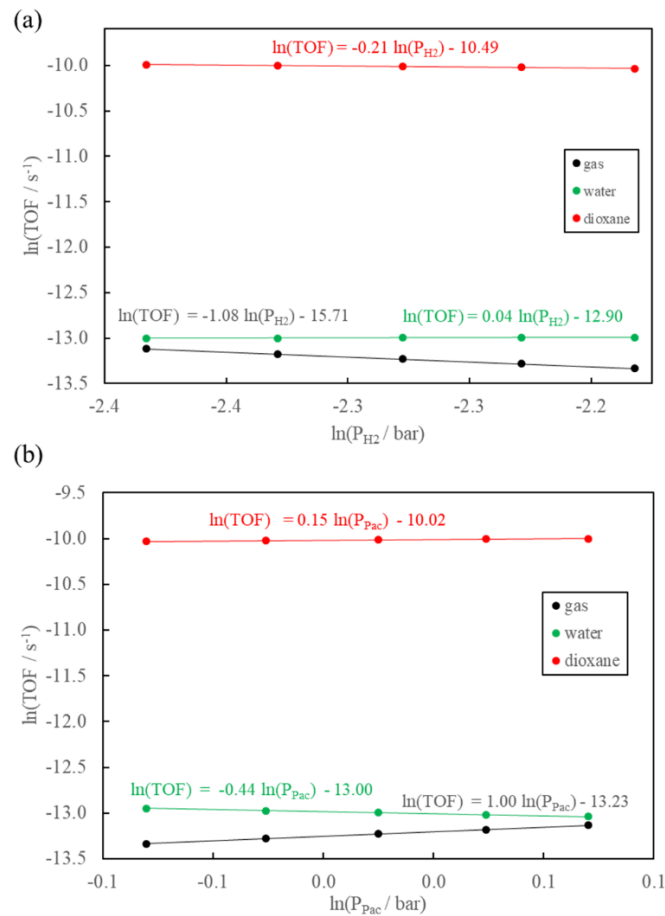


Figure 4 Reaction orders of (a) H₂ and (b) propionic acid at a temperature of 473 K, a propionic acid gas phase partial pressure of 1 bar, a CO gas phase partial pressure of 0.001 bar and a hydrogen partial pressure of 0.1 bar.

Finally, Figure 6 displays Arrhenius plots for the consumption of propionaldehyde in various reaction environments. We compute apparent activation barriers of 0.99 eV, 1.28 eV and 3.03 eV in the gas phase, and liquid 1,4-dioxane and water, respectively. The large apparent activation barrier in water can again be explained by propionic acid inhibition at low temperatures which disappears with increasing temperature when the free site coverage increases (see Table 2 and the change in reaction order with respect to propionic acid as displayed in Figure 4c).

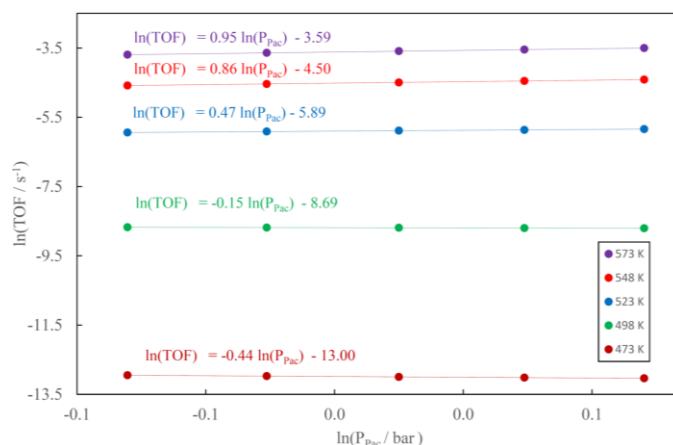


Figure 5 Reaction orders of propionic acid at a temperature of 473 K, a propionic acid gas phase partial pressure of 1 bar, a CO gas phase partial pressure of 0.001 bar and a hydrogen partial pressure of 0.1 bar at various temperatures over Pt (111) in liquid water.

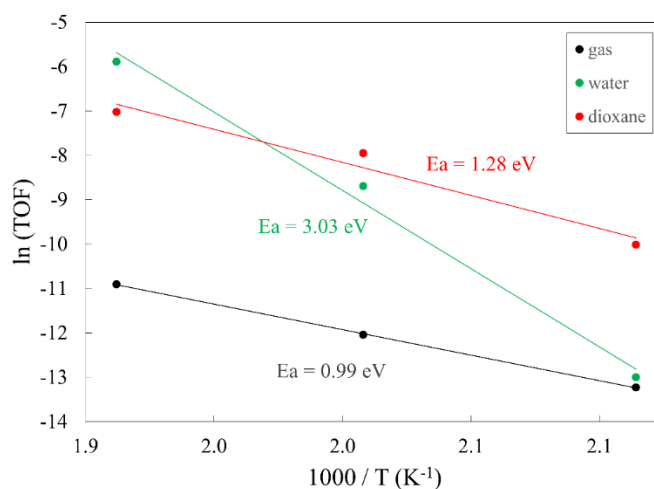


Figure 6 Arrhenius plot for the HDO of propionic acid in the temperature range 473–523 K with a propionic acid gas phase partial pressure of 1 bar, a CO gas phase partial pressure of 0.001 bar and a hydrogen partial pressure of 0.1 bar.

4 Conclusions

Microkinetic models based on transition state theory and DFT have been developed for the investigation of the HDO of propionic acid over Pt (111) surface under both vapor and liquid phase

conditions. In all reaction environments, decarboxylation is not favored. In the gas phase, both decarbonylation products and propanol and propionaldehyde can be produced. However, propanol and propionaldehyde production is favored over decarbonylation products in liquid phase. Under both vapor and liquid phase conditions, the dominant pathway for decarbonylation is the direct path which starts with dehydroxylation of adsorbed propionic acid, followed by α -carbon dehydrogenation and then either direct decarbonylation or further dehydrogenation prior to decarbonylation. Propanol and propionaldehyde production also favor a direct formation pathway which starts with direct dehydroxylation and hydrogenation of the carbonyl group. Only the propionaldehyde production mechanism changes in liquid phase. Here, the propanol production is significantly favored such that propionaldehyde is primarily produced from dehydrogenated surface alcohol species. In liquid 1,4-dioxane and at 473 K, the conversion rate of propionic acid is predicted to increase by one order of magnitude. Higher temperatures further increase the solvent acceleration on the turnover frequency. In liquid water and at 473 K, the propionic acid consumption rate is not significantly increased, primarily because of strong adsorption of propionic acid which leads to the surface being partially blocked by propionic acid. With increasing temperature, however, the TOF is dramatically increased in liquid water and becomes even larger than that in liquid 1,4-dioxane as the surface is much less covered by propionic acid at these temperatures. The rate of the reaction is solely controlled by the dehydroxylation of adsorbed propionic acid under both vapor and liquid phase conditions. The rate of the decarbonylation mechanism is barely affected by the solvents and the increase in propionic acid conversion due to the presence of a solvent primarily originates from an increase in the rate of propanol and propionaldehyde production. Thus, solvents can be designed to manipulate the selectivity of the HDO of organic acids.

ACKNOWLEDGMENTS

We gratefully acknowledge financial support from the U.S. Department of Energy, Office of Basic Energy Science, Catalysis Science program under Award DE-SC0007167 (most of the liquid phase calculations and models and some of the gas phase data) and the National Science Foundation under Grant No. DMREF-1534260 (some of the gas phase data and models). J.Q.B. acknowledges financial support from the National Science Foundation DMREF-1534269. Computational resources have been provided by the National Energy Research Scientific Computing Center (NERSC) which is supported by the Office of Science of the U.S. Department

of Energy and in part by XSEDE under grant number TG-CTS090100. Computational resources from CASCADE cluster from Environmental Molecular Sciences Laboratory (EMSL) under Pacific Northwest National Laboratory (PNNL) are also used for the DFT calculations. Finally, computing resources from the USC High Performance Computing Group are gratefully acknowledged. We also gratefully thank the Writing Center of the University of South Carolina for providing suggestions in preparing this paper.

Appendix A. Supplementary material

The corresponding results of the solvent calculations with a $\pm 10\%$ of the default COSMO Pt cavity radius, including the reaction energies, activation barriers, MKM results, reaction orders of hydrogen and propionic acid etc. are provided. Also shown are the CO and H lateral interaction coefficients of various surface intermediates and the degrees of thermodynamic selectivity control of various key species under various reaction conditions. Finally, a convergence plot of our solvent cluster model is provided.

Appendix B. Supplementary material

The corresponding optimized coordinates of all ground and transition state structures are provided in txt file format.

REFERENCES

- [1] J.N. Chheda, G.W. Huber, J.A. Dumesic, Liquid-phase catalytic processing of biomass-derived oxygenated hydrocarbons to fuels and chemicals, *Angew Chem Int Ed Engl*, 46 (2007) 7164-7183.
- [2] D.C. Elliott, Historical developments in hydroprocessing bio-oils, *Energ Fuel*, 21 (2007) 1792-1815.
- [3] G. Knothe, Dependence of biodiesel fuel properties on the structure of fatty acid alkyl esters, *Fuel Processing Technology*, 86 (2005) 1059-1070.
- [4] M.J. Ramos, C.M. Fernandez, A. Casas, L. Rodriguez, A. Perez, Influence of fatty acid composition of raw materials on biodiesel properties, *Bioresour Technol*, 100 (2009) 261-268.
- [5] G.W. Huber, P. O'Connor, A. Corma, Processing biomass in conventional oil refineries: Production of high quality diesel by hydrotreating vegetable oils in heavy vacuum oil mixtures, *Applied Catalysis A: General*, 329 (2007) 120-129.
- [6] J. Regalbuto, An NSF perspective on next generation hydrocarbon biorefineries, *Computers & Chemical Engineering*, 34 (2010) 1393-1396.
- [7] J. Wildschut, F.H. Mahfud, R.H. Venderbosch, H.J. Heeres, Hydrotreatment of Fast Pyrolysis Oil Using Heterogeneous Noble-Metal Catalysts, *Industrial & Engineering Chemistry Research*, 48 (2009) 10324-10334.
- [8] D. Kubička, P. Šimáček, N. Žilková, Transformation of Vegetable Oils into Hydrocarbons over Mesoporous-Alumina-Supported CoMo Catalysts, *Topics in Catalysis*, 52 (2008) 161-168.
- [9] J. Lu, S. Behtash, A. Heyden, Theoretical Investigation of the Reaction Mechanism of the Decarboxylation and Decarbonylation of Propanoic Acid on Pd(111) Model Surfaces, *The Journal of Physical Chemistry C*, 116 (2012) 14328-14341.
- [10] S. Behtash, J. Lu, M. Faheem, A. Heyden, Solvent effects on the hydrodeoxygenation of propanoic acid over Pd(111) model surfaces, *Green Chem.*, 16 (2014) 605-616.

- [11] S. Behtash, J. Lu, C.T. Williams, J.R. Monnier, A. Heyden, Effect of Palladium Surface Structure on the Hydrodeoxygenation of Propanoic Acid: Identification of Active Sites, *The Journal of Physical Chemistry C*, 119 (2015) 1928-1942.
- [12] J.M. Lu, S. Behtash, M. Faheem, A. Heyden, Microkinetic modeling of the decarboxylation and decarbonylation of propanoic acid over Pd(111) model surfaces based on parameters obtained from first principles, *Journal of Catalysis*, 305 (2013) 56-66.
- [13] J.M. Lu, M. Faheem, S. Behtash, A. Heyden, Theoretical investigation of the decarboxylation and decarbonylation mechanism of propanoic acid over a Ru(0001) model surface, *Journal of Catalysis*, 324 (2015) 14-24.
- [14] S. Behtash, J. Lu, O. Mamun, C.T. Williams, J.R. Monnier, A. Heyden, Solvation Effects in the Hydrodeoxygenation of Propanoic Acid over a Model Pd(211) Catalyst, *The Journal of Physical Chemistry C*, 120 (2016) 2724-2736.
- [15] Y.Q. Chen, D.J. Miller, J.E. Jackson, Kinetics of aqueous-phase hydrogenation of organic acids and their mixtures over carbon supported ruthenium catalyst, *Industrial & Engineering Chemistry Research*, 46 (2007) 3334-3340.
- [16] H. Wan, R.V. Chaudhari, B. Subramaniam, Catalytic Hydroprocessing of p-Cresol: Metal, Solvent and Mass-Transfer Effects, *Topics in Catalysis*, 55 (2012) 129-139.
- [17] J. Lu, S. Behtash, O. Mamun, A. Heyden, Theoretical Investigation of the Reaction Mechanism of the Guaiacol Hydrogenation over a Pt(111) Catalyst, *ACS Catalysis*, 5 (2015) 2423-2435.
- [18] M. Faheem, M. Saleheen, J. Lu, A. Heyden, Ethylene glycol reforming on Pt(111): first-principles microkinetic modeling in vapor and aqueous phases, *Catalysis Science & Technology*, 6 (2016) 8242-8256.
- [19] W.R.M.A. Vannice, Acetic Acid Hydrogenation over Supported Platinum Catalysts, *Journal of Catalysis*, 192 (2000) 322-334.
- [20] H. Olcay, L. Xu, Y. Xu, G.W. Huber, Aqueous-Phase Hydrogenation of Acetic Acid over Transition Metal Catalysts, *ChemCatChem*, 2 (2010) 1420-1424.
- [21] Y.K. Lugo-José, J.R. Monnier, C.T. Williams, Gas-phase, catalytic hydrodeoxygenation of propanoic acid, over supported group VIII noble metals: Metal and support effects, *Applied Catalysis A: General*, 469 (2014) 410-418.
- [22] S. Behtash, J. Lu, E. Walker, O. Mamun, A. Heyden, Solvent effects in the liquid phase hydrodeoxygenation of methyl propionate over a Pd(1 1 1) catalyst model, *Journal of Catalysis*, 333 (2016) 171-183.
- [23] M. Faheem, S. Suthirakun, A. Heyden, New Implicit Solvation Scheme for Solid Surfaces, *The Journal of Physical Chemistry C*, 116 (2012) 22458-22462.
- [24] M. Arend, T. Nonnen, W.F. Hoelderich, J. Fischer, J. Groos, Catalytic deoxygenation of oleic acid in continuous gas flow for the production of diesel-like hydrocarbons, *Applied Catalysis A: General*, 399 (2011) 198-204.
- [25] O. Mamun, M. Saleheen, J.Q. Bond, A. Heyden, Investigation of solvent effects in the hydrodeoxygenation of levulinic acid to γ -valerolactone over Ru catalysts, *Journal of Catalysis*, 379 (2019) 164-179.
- [26] G. Kresse, J. Hafner, Ab initio molecular dynamics for liquid metals, *Phys Rev B Condens Matter*, 47 (1993) 558-561.
- [27] G. Kresse, J. Furthmuller, Efficiency of ab-initio total energy calculations for metals and semiconductors using a plane-wave basis set, *Comp Mater Sci*, 6 (1996) 15-50.
- [28] G. Kresse, D. Joubert, From ultrasoft pseudopotentials to the projector augmented-wave method, *Physical Review B*, 59 (1999) 1758-1775.
- [29] J.P. Perdew, Y. Wang, Accurate and simple analytic representation of the electron-gas correlation energy, *Phys Rev B Condens Matter*, 45 (1992) 13244-13249.
- [30] J.P. Perdew, W. Yue, Accurate and simple density functional for the electronic exchange energy: Generalized gradient approximation, *Phys Rev B Condens Matter*, 33 (1986) 8800-8802.
- [31] W.P. Davey, Precision Measurements of the Lattice Constants of Twelve Common Metals, *Physical Review*, 25 (1925) 753-761.
- [32] H.J. Monkhorst, J.D. Pack, Special points for Brillouin-zone integrations, *Physical Review B*, 13 (1976) 5188-5192.
- [33] G. Henkelman, B.P. Uberuaga, H. Jonsson, A climbing image nudged elastic band method for finding saddle points and minimum energy paths, *Journal of Chemical Physics*, 113 (2000) 9901-9904.
- [34] G. Henkelman, H. Jonsson, A dimer method for finding saddle points on high dimensional potential surfaces using only first derivatives, *Journal of Chemical Physics*, 111 (1999) 7010-7022.
- [35] R.A. Olsen, G.J. Kroes, G. Henkelman, A. Arnaldsson, H. Jonsson, Comparison of methods for finding saddle points without knowledge of the final states, *J Chem Phys*, 121 (2004) 9776-9792.

- [36] A. Heyden, A.T. Bell, F.J. Keil, Efficient methods for finding transition states in chemical reactions: comparison of improved dimer method and partitioned rational function optimization method, *J Chem Phys*, 123 (2005) 224101.
- [37] T.S. Tomoshige Nitta, Masayuki Kuro-oka, Takashi Katayama, AN ADSORPTION ISOTHERM OF MULTI-SITE OCCUPANCY MODEL FOR HETEROGENEOUS SURFACE, *JOURNAL OF CHEMICAL ENGINEERING OF JAPAN*, 17 (1984) 39-45.
- [38] I. Chorkendorff, J.W. Niemantsverdriet, *Concepts of modern catalysis and kinetics*, Wiley-VCH, Weinheim, 2005.
- [39] S.C. Ammal, A. Heyden, Understanding the Nature and Activity of Supported Platinum Catalysts for the Water–Gas Shift Reaction: From Metallic Nanoclusters to Alkali-Stabilized Single-Atom Cations, *ACS Catalysis*, 9 (2019) 7721-7740.
- [40] E.A. Walker, D. Mitchell, G.A. Terejanu, A. Heyden, Identifying Active Sites of the Water–Gas Shift Reaction over Titania Supported Platinum Catalysts under Uncertainty, *ACS Catalysis*, 8 (2018) 3990-3998.
- [41] J.C. Lee, Y. Xu, G.W. Huber, High-throughput screening of monometallic catalysts for aqueous-phase hydrogenation of biomass-derived oxygenates, *Applied Catalysis B-Environmental*, 140 (2013) 98-107.
- [42] C.T. Campbell, The Degree of Rate Control: A Powerful Tool for Catalysis Research, *ACS Catalysis*, 7 (2017) 2770-2779.
- [43] C.T. Campbell, Finding the Rate-Determining Step in a Mechanism, *Journal of Catalysis*, 204 (2001) 520-524.
- [44] V. Pallassana, M. Neurock, Reaction Paths in the Hydrogenolysis of Acetic Acid to Ethanol over Pd(111), Re(0001), and PdRe Alloys, *Journal of Catalysis*, 209 (2002) 289-305.